Received: 8 November 2023 | Revised: 7 February 2024 | Accepted: 9 March 2024

DOI: 10.1002/jev2.12427

RESEARCH ARTICLE

The small extracellular vesicle-mediated intercellular transformation of CXCR1^{Low} to CXCR1^{High} tumour cells promotes the progression of head and neck squamous cell carcinoma

Qiaoshi Xu | **Aoming Cheng** | **Bo Li** | **Xutengyue Tian** | **Zhengxue Han** | **Zhien Feng**

Department of Oral and Maxillofacial-Head and Neck Oncology, Beijing Stomatological Hospital, Capital Medical University, Beijing, China

Correspondence
Zhien Feng and Zhengxue Han. Department of Oral and Maxillofacial-Head and Neck Oncology, Beijing Stomatological Hospital, Capital Medical University, No. 4 Tian Tan Xi Li, Dongcheng District, Beijing 100050, China.
Email: jyfzhen@126.com and hanfl1989@hotmail.com

Funding information
Beijing Science and Technology Commission, Grant/Award Number: Z221100007422046; Beijing Municipal Administration of Hospitals' Youth Programme, Grant/Award Number: QML20231507; Beijing Nova Program, Grant/Award Number: 20230484404; National Natural Science Foundation of China, Grant/Award Number: 82072984; Beijing Hospitals Authority Clinical medicine Development of special funding support, Grant/Award Number: YGLX202338; Beijing Stomatological Hospital, Capital Medical University Young Scientist Program, Grant/Award Number: YSP202111

Abstract

The heterogeneity of tumour cells enables cancers to dynamically adapt to microenvironmental stresses during progression. However, the mechanism underlying the transformation and intercellular communication between heterogeneous tumour cells has remained elusive. Here, we report a "contagion model" that mediates intercellular transformation between heterogeneous tumour cells which facilitates tumour progression. Initially identifying heterogeneous expression of CXCR1, a receptor for interleukin-8, in head and neck squamous cell carcinoma (HNSCC) tumour cells, we found that CXCR1^{High} tumour cells had higher abilities for migration and invasion. Following interleukin-8-mediated activation, CXCR1^{High} cells transformed CXCR1^{Low} cells into CXCR1^{High} cells through the secretion of small extracellular vesicles (sEVs), which increased the proportion of CXCR1^{High} cells and facilitated tumour progression. Mechanistically, we demonstrate that sEVs derived from interleukin-8-activated CXCR1^{High} cells contain high levels of ATP citrate lyase (ACLY), which acetylates NF-κB p65 and facilitates its nuclear translocation to transcribe CXCR1 in CXCR1^{Low} cells. That process could be inhibited by Bempedoic acid, an FDA-approved ACLY-targeted drug. Taken together, our study reveals an sEV-mediated transformation of CXCR1^{Low} to CXCR1^{High} cells that promotes HNSCC progression. This provides a new paradigm to explain the dynamic changes of heterogeneous tumour cells, and identifies Bempedoic acid as a potential drug for HNSCC treatment.

KEYWORDS
ATP-citrate lyase, C-X-C motif chemokine receptor 1, head and neck squamous cell carcinoma, heterogeneity, small extracellular vesicles

1 | INTRODUCTION

Head and neck squamous cell carcinoma (HNSCC) is a common type of cancer that causes great physical and psychological damage to patients (Johnson et al., 2020; Mody et al., 2021). To date, the outcome of HNSCC is still unsatisfactory despite the use of targeted therapies (Cramer et al., 2019; Vathiotis et al., 2021). Accumulating evidence has revealed that the heterogeneity of HNSCC cells is closely related to its treatment failure (Dagogo-Jack & Shaw, 2018; Leemans et al., 2018; Wang et al., 2021). As a hallmark of cancer, heterogeneity has been demonstrated to be in a dynamic status of change and helps to meet the demands of rapid tumour growth (Qian et al., 2022; Sun et al., 2021). Recent studies have found that tumour cells with more active malignant behaviours among the heterogeneous tumour cell population eventually become the majority and form the dominant subset in

the tumour microenvironment (TME) to promote tumour progression (Hanahan, 2022). However, how the dominant subset forms and the underlying mechanism behind that process is still unknown.

Emerging evidence has revealed that heterogeneous tumour cells can influence each other through intercellular signalling and promote the progression of tumours (Attaran & Bissell, 2021; Jiang et al., 2022). Small extracellular vesicles (sEVs) act as couriers for substance transport between cells and play a vital role in this process (Dai et al., 2020; van Niel et al., 2022). sEVs as cell-secreted products carry abundant amounts of bioactive substances including proteins, lipids, and nucleic acids, and the contents of sEVs are highly regulated by the type of cells producing them (Kalluri & LeBleu, 2020). Therefore, sEVs hold important biological information from heterogeneous cells that could reshape the TME and promote tumour progression (Ludwig et al., 2022; Yin et al., 2022). In this case, the role of sEVs in tumour progression induced by intercellular communication is worth deeper investigation.

Here, we propose a "contagion model" that interprets the formation of a dominant subset of tumour cells through intercellular communications between heterogeneous tumour cells mediated by sEVs. Our previous study has recently proven the pro-tumour effect of interleukin-8 (IL-8), which exists in abundance in the TME of HNSCC (Xu et al., 2020), and discovered the heterogeneity of responses of different HNSCC cells to IL-8 during last experiments. In the current study, we identify the heterogeneous expression of C-X-C motif chemokine receptor 1 (CXCR1), a receptor for IL-8, in HNSCC tumour cells and show that $CXCR1^{High}$ cells have higher abilities for migration and invasion. Moreover, upon IL-8-mediated activation, $CXCR1^{High}$ cells transformed $CXCR1^{Low}$ cells into $CXCR1^{High}$ cells and eventually became the dominant subset to promote tumour progression. Mechanistically, sEVs derived from IL-8-activated $CXCR1^{High}$ cells carried ATP citrate lyase (ACLY) into $CXCR1^{Low}$ cells to acetylate Nuclear Factor-Kappa B (NF-κB) p65 thus promoting its nuclear translocation and the subsequent transcription of CXCR1. Importantly, that process could be inhibited by the only FDA-approved ACLY-targeted drug Bempedoic acid (BA). The results of this study not only uncover the underlying molecular mechanism of ACLY promoting CXCR1 expression, but more importantly, we provide a novel direction for understanding the communication between heterogeneous tumour cells and its effect on tumour progression, and prove that BA is a potential targeted drug for HNSCC treatment.

2 | MATERIALS AND METHODS

2.1 | Ethics statement

This study was approved by the Institutional Review Board of the Beijing Stomatological Hospital of Capital Medical University (Beijing, China). Informed consent was signed by all patients enrolled. Animal studies were performed following the NIH Guide for the Care and Use of Laboratory Animals, with the approval of the Institute Animal Care and Use Committee of the Beijing Stomatological Hospital of Capital Medical University.

2.2 | Patients and specimens

A total of 48 patients diagnosed with HNSCC and three patients diagnosed with epithelium dysplasia who were treated in the Department of Oral and Maxillofacial-Head and Neck Oncology, Beijing Stomatological Hospital, Capital Medical University were enrolled in this study. All patients enrolled were diagnosed as HNSCC by biopsy in the outpatient clinic and did not subject to any treatment prior to the resection of primary tumour. Tissue samples were obtained instantly after the tumours were entirely removed, and medical records of enrolled patients were collected after discharge for further analysis. The cases of HNSCC were staged according to the 8^{th} edition of the Union for International Cancer Control/American Joint Committee on Cancer (UICC/AJCC) classification system. The baseline demographics of patients enrolled are summarized in Tables S1 and S2.

2.3 | Cell culture

Normal human oral keratinocyte (HOK) cells, four HNSCC cell lines (HN4, HN6, Cal27 and HN30) and HEK 293T cells were used in this study. HN4, HN6 and HN30 cell lines were kindly provided from the Shanghai Ninth People's Hospital, Shanghai, China. Cal27 and HEK 293T cell lines were purchased from American Type Culture Collection (ATCC, USA). HOK cells were purchased from ScienCell Research Laboratories (USA). All cells were cultured in Dulbecco's modified Eagle's medium (DMEM; Gibco, USA) supplemented with 10% exosome-depleted foetal bovine serum (FBS; A27208-03, Gibco), 100 U/mL penicillin and 100 μg/mL streptomycin at 37°C in a standard humidified atmosphere of 5% CO_2. It is worth mentioning that to simulate the high IL-8 concentration environment inside HNSCC tumour, recombinant human IL-8 (Peprotech, USA) was added to the medium in all in vitro assays except assays that tested the function of IL-8 (shown in Figure S1A-D, Figure S2A, B). According to our previous research, we used 100 ng/mL IL-8 as an appropriate concentration for this exogenous stimulation (Xu et al., 2020).

GW4869 (HY-19363, MedChemexpress (MCE), USA) was used to verify the function of sEVs at a concentration of 10 μM. To determine the function of sEVs or its content, sEVs (50 μg) derived from HNSCC cells were co-cultured with HN6 cells for 24 h before further experiments were conducted. BA was applied at the concentration indicated by the survival assay to treat HN6 cells for 24 h.

2.4 | Transfection of siRNAs and plasmids

Plasmids and the small interfering RNA (siRNA) targeting ACLY were designed and synthesized by RiboBio (China). pcDNA3.1-EF1a-mcherry-CMV-MCS-3XFlag-SV40promoter-neo was used as the vector for ACLY overexpression. Plasmids and si-ACLY as well as the empty vector and the scrambled sequence were transfected into HNSCC cells using Lipofectamine™ 3000 (Invitrogen, USA) following the manufacturer's instructions. The sequence of si-ACLY is as follows: #1, 5′-CGAUACCAUCUGUGAUCUA-3′; #2, 5′-UUCUUGAUCAGCUUUCUCGUGAGGG-3′.

2.5 | RNA extraction and qRT-PCR analysis

RNA was extracted from tissues and cells using TRIzol reagent (Invitrogen). qRT-PCR was performed following the manufacturer's instructions and as described in our previous study (Xu et al., 2020). The primers for CXCR1 and GAPDH were synthesized by Sangon Biotech (China) and the sequences were as follows: CXCR1-F: 5′-GGGATTTCTCCATAGCTGCCT-3′; CXCR1-R: 5′-ACAGACGAAGAAGTGTAGGAGG-3′; GAPDH-F: 5′-CCTCTGACTTCAACAGCGAC-3′; GAPDH-R: 5′-TCCTCTTGTGCTCTTGCTGG-3′.

2.6 | Cellular proliferation, migration and invasion assays

Wound healing assays were performed to detect the migration ability of HNSCC cells. Transwell assays including uncoated inserts and Matrigel-coated inserts were used separately to determine migration and invasion abilities. The proliferation ability was determined using Cell Counting Kit 8 (CCK8) assays (Dojindo, Japan). Finally, colony-forming abilities were compared by the number of clusters formed by 1000 cells incubated for 10–14 days. These experiments were performed as described in our previous study and were all repeated three times (Xu et al., 2020).

2.7 | Hematoxylin-eosin (H&E) and immunohistochemistry (IHC) staining

A standard H&E staining was performed to identify the pathological type of lung metastasis nodes formed in the animal study. IHC analysis was performed to detect the expression of CXCR1 and ACLY in human HNSCC samples and xenograft tumours. The IHC procedure was performed as described before (Xu et al., 2020). The primary antibodies used were CXCR1 (ab124344, abcam, USA, dilution 1:200) and ACLY (ab126129, abcam, dilution 1:200). The intensity of staining was scored as follows: 0 = negative, absence of stained cells; 1 = weak; 2 = moderate; and 3 = strong. The IHC staining score was calculated by multiplying the percentage of positive cells by the staining intensity. The scoring was conducted by researchers who were blind to the group information of xenograft tumours or the clinical data of patients.

2.8 | Immunofluorescence and fluorescence analysis

HNSCC cells were harvested from the glass coverslips and were fixed in 4% paraformaldehyde. After sealing with 10% normal goat serum for 1 h, the primary antibodies were applied and incubated overnight at 4°C. Secondary antibodies conjugated with rhodamine or FITC (Cell Signalling Technology (CST), USA, dilution 1:200) were incubated on the next day and Vectashield mounting medium containing 4′,6-diamidino-2-phenylindole (DAPI) (Sigma-Aldrich, USA) was then applied. To detect the expression and localization of p65, Triton X-100 (Sigma-Aldrich) was applied before sealing with goat serum. The primary antibodies used were CXCR1 (ab313462, abcam, dilution 1:50) and p65 (#8242, CST, dilution 1:400).

To visualize the phagocytosing process of sEVs, we used PKH26 to stain HN6 cells and Carboxyfluorescein N-succinimidyl ester (CFSE, No. E607337, Sangon Biotech) to stain sEVs according to the manufacturer's instructions. CFSE-labelled sEVs and PKH26-labelled HN6 cells were co-cultured for 4 h to observe the fluorescence status. Immunofluorescence and fluorescence images were captured using a fluorescence microscope (Olympus, Japan).

2.9 | Flow cytometry

Tissue samples were harvested and processed into single-cell suspensions. After incubation with antibodies for 20 min on ice, the suspensions were evaluated using a flow cytometer. The antibodies used were CD326 (#751942, BD Biosciences, USA) and CXCR1 (#551081, BD Biosciences). The results were analysed by FlowJo™ software (ver. 10.4.0., USA).

2.10 | Isolation and identification of sEVs

HNSCC cells (HN4, HN6, and Cal27) with or without transfection of plasmids or si-RNA targeting ACLY were cultured for 48 h to prepare sEVs. The supernatants were centrifuged at 3000×g for 15 min to remove cell debris, passed through a 0.22 μm filter (Millipore, USA) and centrifuged at 100,000×g for 70 min. The pellets were washed with phosphate buffered saline (PBS) and the sEVs were obtained after centrifugation at 100,000×g for 70 min. Finally, the sEVs were identified using transmission electron microscopy, nanoparticle tracking analysis and western blot (HSP70, TSG101, CD9).

2.11 | LC-MS/MS-based proteomics

To identify the specific contents of sEVs derived from $CXCR1^{High}$ and from $CXCR1^{Low}$ cells that induced this transformation, we isolated sEVs derived from HN4 cells and HN6 cells and analysed them using liquid chromatography-tandem mass spectrometry (LC-MS/MS)-based proteomics. LC-MS/MS analysis was performed using a Q Exactive Plus mass spectrometer (Thermo Fisher Scientific, USA) that was coupled to Easy nLC (Thermo Fisher Scientific). The MS data were analysed using MaxQuant software version 1.6.14.0. The search followed an enzymatic cleavage rule of Trypsin/P and allowed a maximum of two missed cleavage sites and a mass tolerance of 20 ppm for fragment ions. The cutoff of global false discovery rate (FDR) for peptide and protein identification was set to 0.01.

2.12 | Cell lines transcriptome analysis

Transcriptome analysis was performed on HNSCC cell lines (HN4, HN6 and Cal27) cultured with 100 ng/mL IL-8 for 24 h (Figure 4c) or transfected with plasmids containing ACLY (Figure 5a). Specifically, the total RNA were sequenced by the Illumina NovaSeq 6000 (USA). The index of the reference genome was constructed using Hisat2 (v2.0.5). Fragments per kilobase of transcript sequence per million (FPKM) of each gene was calculated based on the length of the gene and the number of reads mapped to that gene. Finally, differential expression analysis of the two groups was performed using the DESeq2 R package (1.20.0). The resulting P-values were adjusted using the Benjamini and Hochberg approach to control for false discovery rate. Padj ≤ 0.05 and $|\log2(\text{foldchange})| \geq 1$ were set as the threshold for significant differential expression.

2.13 | Western blot analysis

Proteins derived from sEVs, nucleus and cytoplasm of HNSCC cells as well as total HNSCC cells were collected using sodium dodecyl sulphate lysis buffer (Beyotime, China). The cell lysates (20 μg) were electrophoresed using polyacrylamide gel and transferred to polyvinylidene fluoride (PVDF) membranes (Merck Millipore, USA). After blocked with nonfat milk for 1 h at room temperature, the membranes were incubated with primary antibodies overnight at 4°C. The membranes were incubated with secondary antibodies on the second day and visualized with ECL Ultra (New Cell and Molecular Biotech, China). GAPDH and HSP90 were used as loading control. The antibodies used including: CXCR1 (ab124344, abcam, dilution 1:1000), ACLY (ab126129, abcam, dilution 1:1000), p65 (#8242, CST, dilution 1:1000), ac-p65 (ab218533, abcam, dilution 1:1000), GAPDH (#5174, CST, dilution 1:1000), H3 (#4499, CST, dilution 1:2000) and HSP90 (#4877, CST, dilution 1:1000). Densitometric values for all western blot experiments were analysed using software ImageJ and the results were uploaded as Supplementary file.

2.14 | Dual-luciferase reporter assay

HEK 293T cells transfected with vector containing CXCR1 promoter region in the control, wild type and mutant group for 48 h. A dual-luciferase reporter assay kit (Beyotime, China) was used according to the manufacturer's instructions to verify the promoter activities.

2.15 | Chromatin immunoprecipitation (ChIP) assays

ChIP assays were performed on HN4 cells using a SimpleChIP Enzymatic Chromatin IP kit (#9003, CST). IgG was used as the negative control. An anti-ac-p65 antibody (ab218533, abcam) was used to pull down the target genes in the promoter regions. ChIP DNAs were analysed using qPCR and were normalized to the input data. The primers targeting the CXCR1 promoter region were as follows: NC-F: 5′-GTTGTGGAAGGTGGAGAA-3′; NC-R: 5′-CAAGGATGTGAGAGCAGT-3′; Motif1-F: 5′-GTGACGAAGGTGCCAGAA-3′; Motif1-R: 5′-AGCAGAGAGACCACAGAGC-3′; Motif2-F: 5′- GACTATTTTCTGCCCTTG-3′ and Motif2-R: 5′-AGTTGTGCTTTCCTCCTG-3′.

2.16 | Animal experiments

Six-week-old BALB/c male nude mice were bred in SPF facilities and were used for the in vivo assays. The mice were blindly grouped and each group contained five mice. To simulate the high IL-8 concentration environment inside HNSCC tumour, IL-8 was injected (0.5 mg/kg, s.c.) every other day in every group of the in vivo studies except assays that tested the function of IL-8 (shown in Figure S1E-H). According to our results, we used HN4 cells as $CXCR1^{High}$ cells and HN6 cells as $CXCR1^{Low}$ cells for the formation of heterogeneous tumours and lung metastasis nodes. For tumourigenicity assays, 1×10^6 HN4 cells or HN6 cells were injected into the right flanks of mice to form tumours. For lung metastasis assays, 1×10^6 HN4 cells or HN6 cells were injected through the lateral tail vein in separate mice. The volume of each xenograft tumour was measured every week and all mice were euthanized at the end of the fifth week. Lung tissues with metastasis nodes were fixed in Bouin's fixative diluted 1:5 with neutral-buffered formalin for nodule observation (Xu et al., 2020). All tumours were collected for the measurement of volume, weight and IHC staining.

To evaluate the effect of $CXCR1^{High}$ cells to transform $CXCR1^{Low}$ cells, we injected 5×10^5 HN4 cells mixed with 5×10^5 HN6 cells in the mixed group in addition to the HN4 and HN6 groups, which were constructed using the method described above (shown in Figure 3a-e). The mice were euthanized at the end of the third, fourth and fifth week to evaluate the transformation of $CXCR1^{Low}$ cells during tumour progression.

To test the functions of sEVs, ACLY and BA in the transformation process, we used 1×10^6 HN6 cells to form xenograft tumours (shown in Figure 3m-p, Figure 4l, m, Figure 7g-k). Considering that the transformation process mediated by sEVs was occurred inside the tumour, 50 μg of sEVs derived from HN4 cells, HN6-vector or HN6-ACLY were injected into the xenograft tumours every other day starting on day 7. Finally, according to previous studies, BA was applied (30 mg/kg, i.p.) once a day.

2.17 | Bioinformatics analysis

The data of CXCR1 expression for HNSCC patients were obtained from the The Cancer Genome Atlas (TCGA) dataset. The clinical data of TCGA HNSCC patients were obtained from cBioportal (http://www.cbioportal.org/). According to the purpose of this study, the enrolled patients with CXCR1 expression level in the lower third were categorized as low level group, the others were categorized as high level group. To analyse the heterogeneity of CXCR1 in HNSCC cells, we selected the publicly available single-cell dataset GSE103322 (Puram et al., 2017) and used the scSTAR method (Hao et al., 2023) to group HNSCC cells according to their CXCR1 expression levels. The JASPAR dataset (https://jaspar.genereg.net/) was used to predict p65 binding sites in the CXCR1 promoter region.

2.18 | Statistical analysis

Statistical analyses were performed using SPSS 22.0, R Studio and GraphPad Prism version 8.0.2 software. Two-tailed unpaired Student's *t*-test and one-way ANOVA were performed to evaluate statistical differences. Survival analysis was performed using the Kaplan–Meier method and log-rank test. Hazard ratio was calculated using Cox proportional hazards model (Enter method). A p value of less than 0.05 (* $p < 0.05$, ** $p < 0.01$, *** $p < 0.001$) is considered statistically significant. Data are presented as means ± SD of three independent experiments.

3 | RESULTS

3.1 | The CXCR1-related heterogeneity of tumour cells correlates with HNSCC progression

To thoroughly understand the role of CXCR1 in HNSCC, we investigated its expression and prognostic value based on data from both TCGA dataset and our clinical samples. Pan-cancer analysis showed that the expression of CXCR1 in HNSCC was not only higher than in normal tissue, but also had the highest level of all cancer types examined (Figure 1a). Kaplan–Meier analysis of 5-year overall survival (OS) proved that a higher expression of CXCR1 is related to worse outcome in HNSCC (Figure 1b, c). These results suggested the important role of CXCR1 in HNSCC. However, the expression of CXCR1 varied from patient to patient (Figure 1d). Our clinical samples showed that HNSCC patients with advanced stage tumours (Figure 1e) or lymph node metastases (Figure 1f) had a significantly higher expression levels of CXCR1, and increased with tumour progression (Figure 1g). The baseline data of patients enrolled were summarized in Table S1.

To further explore the expression of CXCR1 in HNSCC, we used the scSTAR method and analysed the single-cell dataset GSE103322. After identifying and isolating the malignant cells, we grouped them according to their expression level of CXCR1. The results showed that there were heterogeneous subsets related to CXCR1 in HNSCC cells (Figure 1h). Furthermore, we detected the mRNA and protein levels of CXCR1 in normal oral epithelium and different HNSCC cell lines. The results showed that although all HNSCC cell lines had a higher expression of CXCR1 compared with HOK cell line, the CXCR1 level among HNSCC cell lines were significantly different. HN4 cells and Cal27 cells had a significantly higher expression levels of CXCR1 while HN6 cells had the lowest expression level of CXCR1, and HN30 cells was in between (Figure 1i, j). Immunofluorescence staining visualized the high expression level of CXCR1 in HN4 cells and in Cal27 cells while the fluorescence intensity of CXCR1 in HN30 cells was significantly lower and in HN6 cells was barely visible (Figure 1k). Thus, we used HN4 cells and Cal27 cells as $CXCR1^{High}$ cells and HN6 cells as $CXCR1^{Low}$ cells. Considering the intermediate level of CXCR1 in HN30 cells, we excluded this cell line from subsequent experiments to avoid interference. This heterogeneity of CXCR1 expression and its correlation with clinical features were then confirmed in patients' samples. Flow cytometry found that patients with T4N2bM0 tumours had a significantly higher percentage of $CXCR1^{High}$ cells than patients with T1N0M0 tumours (Figure 1l). IHC staining of CXCR1 also showed the increasing proportion of $CXCR1^{High}$ cells from precancerous lesion to advanced-stage HNSCC (Figure 1m). However, the reason for the tumour progression caused by the elevated proportion of $CXCR1^{High}$ cells needed further exploration.

3.2 | $CXCR1^{High}$ cells have more active malignant behaviours and cause HNSCC progression

Previous results uncovered the rising proportion of $CXCR1^{High}$ cells along with the tumour stage in HNSCC. Therefore, we assumed that $CXCR1^{High}$ cells have more active malignant behaviours than $CXCR1^{Low}$ cells and cause the progression of HNSCC. To simulate the high IL-8 concentration environment inside HNSCC tumour, we added 100 ng/mL IL-8 into the medium and assessed the malignant behaviours of $CXCR1^{High}$ and $CXCR1^{Low}$ HNSCC tumour cells. Wound healing assays showed that $CXCR1^{High}$ cells, represented by HN4 cells and Cal27 cells, had a stronger migratory ability (Figure 2a). Transwell assays indicated that $CXCR1^{Low}$ cells, represented by HN6 cells, had significantly fewer cells in the lower chambers with or without matrigel (Figure 2b). Similar results were observed in colony-forming assays, where $CXCR1^{High}$ cells had a higher number of clone clusters than $CXCR1^{Low}$ cells after culture for 7 days (Figure 2c). However, the results of CCK8 assays found that the ability of those different cell types to proliferate was about the same (Figure 2d). This result indicated that the elevated proportion of $CXCR1^{High}$ cells was not due to their greater proliferative ability and outgrow $CXCR1^{Low}$ cells. Moreover, these experiments were conducted on $CXCR1^{High}$ and $CXCR1^{Low}$ HNSCC cells without exogenous IL-8. The results showed no significant difference of malignant behaviours between $CXCR1^{High}$ and $CXCR1^{Low}$ HNSCC cells which indicated that CXCR1 as the receptor of IL-8 mediated the enhancement of migration and invasive abilities (Figure S1A-D).

The in vivo assays confirmed the results above. Tumorigenicity study showed that with the stimulation of IL-8, tumours from HN4 cells grew faster and were significantly larger and heavier than tumours from HN6 cells (Figure 2e-h). Moreover, lung metastasis assay found that HN4 cells formed significantly more metastasis nodes with the injection of IL-8 compared with HN6 cells (Figure 2i). However, there was no significant difference in both tumorigenicity and lung metastasis assays for $CXCR1^{High}$ and $CXCR1^{Low}$ HNSCC cells without IL-8 stimulation (Figure S2E-I). H&E staining was performed to identify the pathological type of lung metastasis nodes (Figure 2j, Figure S1J). IHC staining confirmed the heterogeneous expression of CXCR1 in the HN4 cells and HN6 cells (Figure 2k, Figure S1K). These results proved that with the high concentration of IL-8 in the TME of HNSCC, $CXCR1^{High}$ cells have stronger migration and invasive abilities and were the dominant subset in HNSCC and promoted tumour progression. However, the similarity in the proliferative capacity of $CXCR1^{High}$ and $CXCR1^{Low}$ cells led us to wonder why there was an increasing proportion of $CXCR1^{High}$ cells along with tumour stage.

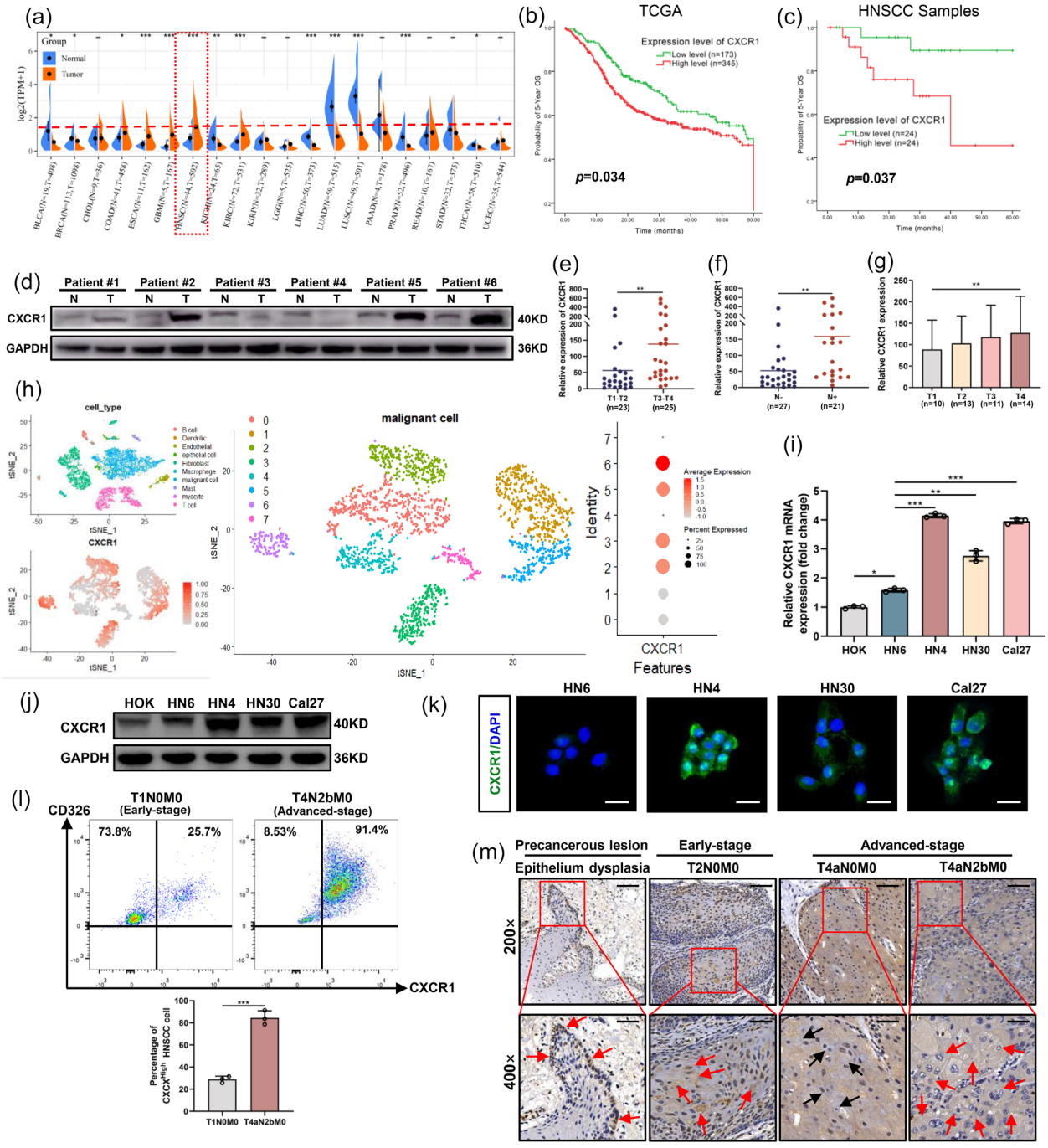

FIGURE 1 **The CXCR1-related heterogeneity of tumour cells correlates with HNSCC progression**. (a) Pan-cancer analysis of the expression of CXCR1. (b, c) Kaplan–Meier analysis of 5-year OS of HNSCC patients with different expression levels of CXCR1 based on TCGA database ($n = 518$, $p = 0.034$, Hazard ratio: 1.285) (b) and clinical samples ($n = 48$, $p = 0.037$, Hazard ratio: 4.607) (c). (d) Western blot analysis of CXCR1 in normal tissues (N) and tumour tissues (T) from HNSCC patients. (e, f) PCR analysis of HNSCC tissue samples ($n = 48$) from patients with different tumour stages (e) or lymph node metastases (f). (g) CXCR1 expression in different stages based on HNSCC tissue sample ($n = 48$). (h) Analysis of single-cell dataset GSE103322 to identify heterogenous subsets of CXCR1 in HNSCC. (i, j) PCR (i) and western blot (j) analysis of CXCR1 level in HOK and HNSCC cell lines. (k) Immunofluorescence staining images to identify CXCR1 level in HN6, HN4, HN30 and Cal27 cells. Green: CXCR1, Blue: DAPI. Scale bars, 50 μm. (l) Flow cytometry analysis of the percentage of $CXCR1^{High}$ tumour cells in T1N0M0 ($n = 3$) and T4N2bM0 ($n = 3$) HNSCC tissue samples. (m) IHC staining of CXCR1 in precancerous lesion (epithelium dysplasia), early-stage (T2N0M0) and advanced-stage (T4aN0M0 and T4aN2bM0) tissue samples. Red arrows indicate $CXCR1^{High}$ cells and black arrows indicate $CXCR1^{Low}$ cells. Scale bars, 50 μm (top row), 25 μm (bottom row). Data are presented as means ± SD (e-h). * $p < 0.05$, ** $p < 0.01$, and *** $p < 0.001$. Data in (b, c) were calculated by Kaplan–Meier analysis and log-rank test; by two-tailed unpaired Student's t-test in (e, f, l); by one-way ANOVA in (g, i).

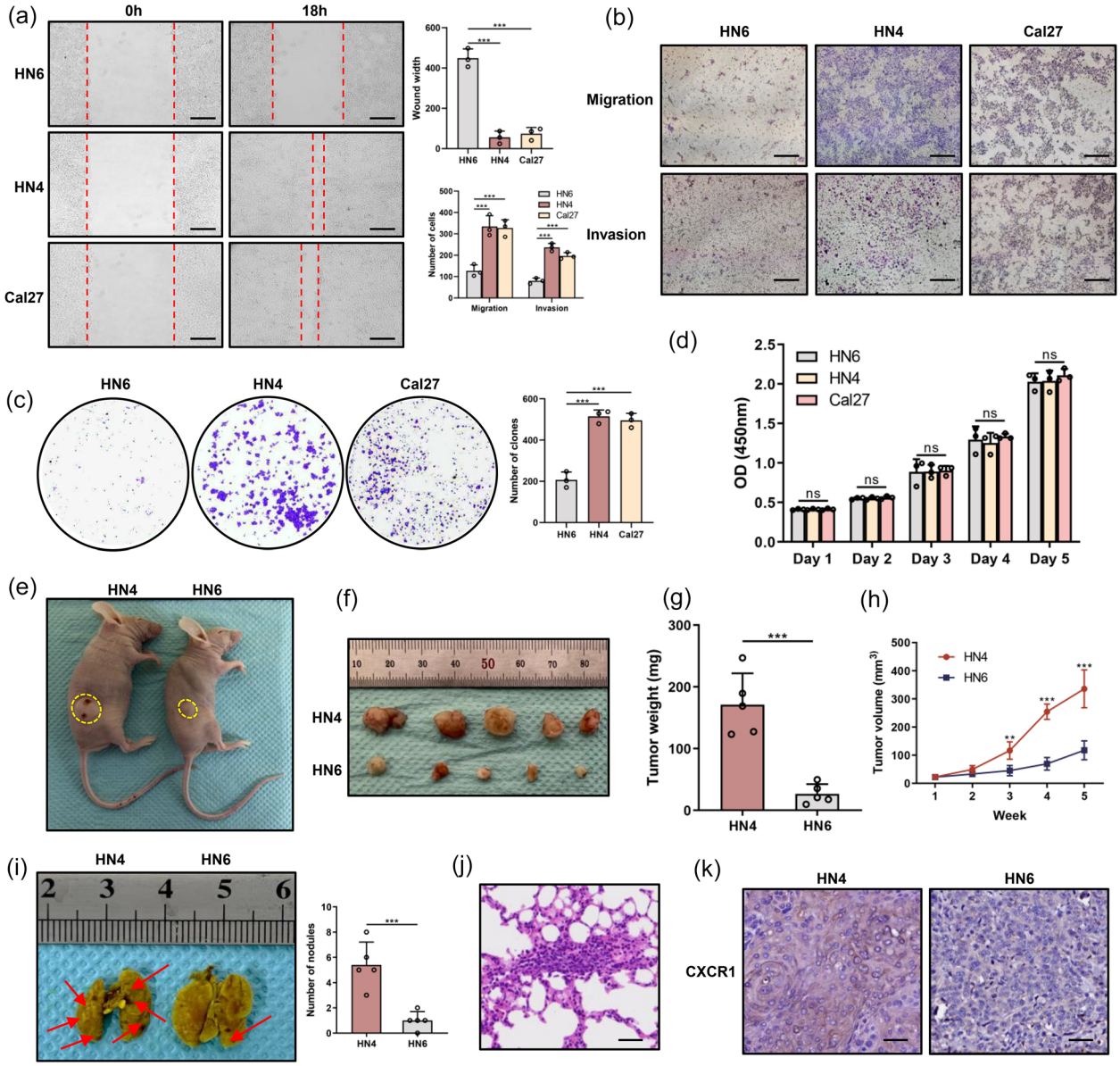

FIGURE 2 **CXCR1^{High} cells have more active malignant behaviours and cause HNSCC progression.** (a) Wound healing assays of CXCR1^{High} cells represented by HN4 cells and Cal27 cells and CXCR1^{Low} cells represented by HN6 cells with the stimulation of IL-8 (100 ng/mL). Scale bars, 100 μm. (b) Migration and invasion abilities of CXCR1^{High} and CXCR1^{Low} cells tested by Transwell assays with the stimulation of IL-8 (100 ng/mL). Scale bars, 100 μm. (c) Colony-forming assays for CXCR1^{High} and CXCR1^{Low} cells stimulated with IL-8 (100 ng/mL). (d) Proliferation ability of CXCR1^{High} and CXCR1^{Low} cells determined by CCK8 assays with the stimulation of IL-8 (100 ng/mL). (e, f) Representative images of xenograft tumours formed by HN4 cells or HN6 cells treated with IL-8 (0.5 mg/kg, s.c. every other day) ($n = 5$). (g, h) Tumour weight (g) and growth curves (h) of HN4 and HN6 groups. (i) Representative image of lung tissues fixed in Bouin's fixative diluted 1:5 with neutral-buffered formalin from HN4 or HN6 group with the injection of IL-8 ($n = 5$). Red arrows indicate metastasis nodes. (j) H&E staining of lung metastasis nodes to identify the pathological type. Scale bars, 50 μm. (k) IHC staining to prove the CXCR1 expression of tumours formed by HN4 cells or HN6 cells. Scale bars, 50 μm. ns, not significant, ** $p < 0.01$, and *** $p < 0.001$. Data in (a–d) were calculated by one-way ANOVA; by two-tailed unpaired Student's t-test in (g, h, i).

3.3 | sEVs derived from CXCR1^{High} cells transform CXCR1^{Low} cells into CXCR1^{High} cells

To further validate the increasing proportion of CXCR1^{High} cells during tumour progression, we established xenograft tumour models using CXCR1^{High} cells (HN4), CXCR1^{Low} cells (HN6) and a mixture of those two types of cells. The xenograft tumours were harvested at the end of 3, 4 and 5 weeks after the injection of tumour cells (Figure 3a). In accord with previous results, tumours in the HN4 group were significantly larger and heavier compared with tumours in the HN6 group. However, tumours in the mixed group showed a gradual acceleration of growth rate (Figure 3b–e). More importantly, an elevated ratio of CXCR1^{High} cells was observed in the mixed group along with tumour progression (Figure 3c). These results directly proved that CXCR1^{High}

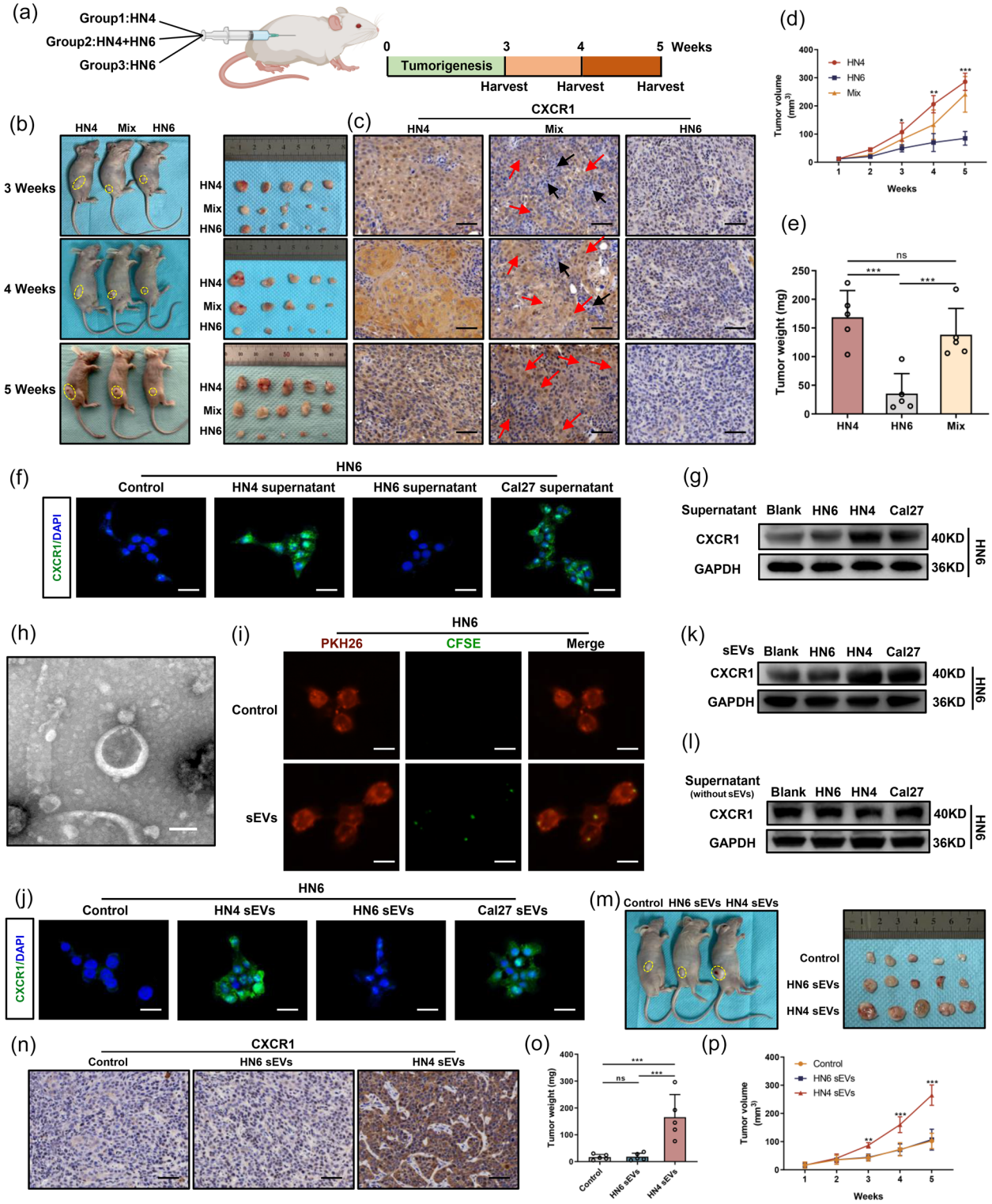

FIGURE 3 **sEVs derived from CXCR1^{High} cells transform CXCR1^{Low} cells into CXCR1^{High} cells.** (a) Schematic diagram of xenograft tumours formed by HN4 cells, HN6 cells or a mix of HN4 and HN6 cells. Tumours were harvested at 3, 4 and 5 weeks to test the transformation of CXCR1^{Low} cells during tumour progression. (b) Xenograft tumours at 3, 4 and 5 weeks in the indicated groups treated with IL-8 (0.5 mg/kg, s.c. every other day) ($n = 5$). (c) IHC staining of CXCR1 in tumours harvested at 3, 4 and 5 weeks of the indicated groups. Red arrows indicate CXCR1^{High} cells and black arrows indicate CXCR1^{Low} cells. Scale bars, 50 μm. (d, e) Growth curves and tumour weights of HN4 group, HN6 group or the mix group. (f) Immunofluorescence images of CXCR1 in HN6 cells treated with CM prepared from the indicated supernatant. Green: CXCR1, Blue: DAPI. Scale bars, 50 μm. (g) Western blot analysis of the expression of CXCR1 in HN6 cells treated with CM prepared by the indicated supernatant. (h) Electron microscopy image of sEVs derived from HNSCC cells. Scale bar, 100 nm. (i) Fluorescence images of CFSE-labelled sEVs phagocytosed by PKH26-labelled HN6 cells after co-cultured for 4 h. Scale bars, 25 μm. (j) CXCR1 immunofluorescence staining of HN6 cells treated with sEVs derived from the indicated cells. Green: CXCR1, Blue: DAPI. Scale bars, 50 μm. (k) Protein level of CXCR1 in HN6 cells after treatment with sEVs derived from the indicated cells. (l) CXCR1 expression in HN6 cells after treatment with CM derived from

(Continues)

FIGURE 3 (Continued)

GW4869 (10 μM) pre-treated HNSCC cells as indicated. (m) Representative images of xenograft tumours formed by HN6 cells and treated with sEVs derived from the indicated cells ($n = 5$). (n) IHC staining of CXCR1 in xenograft tumours treated with sEVs derived from the indicated cells. Scale bars, 50 μm. (o, p) Tumour weights and growth curves of xenograft tumours of the indicated groups. ns, not significant, * $p < 0.05$, ** $p < 0.01$, and *** $p < 0.001$. Data in (d, e, o, p) were calculated by one-way ANOVA.

cells promoted tumour progression by increasing their proportion. Current studies have found that communications between heterogeneous cells promote tumour progression. Combined with our previous results, we speculated that $CXCR1^{High}$ cells might transform $CXCR1^{Low}$ cells through intercellular signalling, resulting in a higher proportion of CXCR1-expressing cells and promoting tumour progression.

To test that hypothesis, we used the supernatants from HN6 cells, HN4 cells and Cal27 cells as conditioned medium (CM) to treat HN6 cells. Immunofluorescence staining showed a significant increase in the fluorescence intensity of CXCR1 in HN6 cells cultured in the CM from $CXCR1^{High}$ cells (Figure 3f). Western blot analysis further validated that result at the protein level (Figure 3g). However, this phenomenon did not occur for CM made without IL-8 treatment (Figure S2A, B). These results indicated that the production of $CXCR1^{High}$ cells mediated the transformation of $CXCR1^{Low}$ cells. sEVs are important couriers for intercellular signalling and might mediate that process. To characterize the role of sEVs in this process, we isolated and identified sEVs derived from HNSCC cells (Figure 3h, Figure S2C, D). CFSE-labelled sEVs were observed inside the cells after co-culture with HN6 cells for 4 h, demonstrating the phagocytosis of sEVs by HNSCC cells (Figure 3i). Our previous experiments were then repeated used sEVs derived from the different HNSCC cell types. The expression of CXCR1 in HN6 cells was also significantly enhanced by treatment with sEVs derived from $CXCR1^{High}$ cells (Figure 3j, k). In addition, we used GW4869 to inhibit the secretion of sEVs and prepared CM from the different types of HNSCC cells. GW4869 significantly reduced the concentration of sEVs in CM (Figure S2E, F). The expression of CXCR1, which was originally enhanced by treatment with the $CXCR1^{High}$ cell supernatant, was not elevated (Figure 3l). Finally, the role sEVs was confirmed by in vivo assays. We used HN6 cells to establish xenograft tumour models, which were treated with sEVs derived from HN6 cells or HN4 cells. The results showed that tumours treated with sEVs derived from HN4 cells were significantly larger and heavier, and had a gradually elevated expression of CXCR1 (Figure 3m-p).

3.4 | ACLY in sEVs derived from $CXCR1^{High}$ cells regulates the transforming process

The results reported above proved that sEVs derived from $CXCR1^{High}$ cells transform $CXCR1^{Low}$ cells to express CXCR1, and the contents of sEVs that regulate that process needed further exploration. To accomplish that, LC-MS/MS-based proteomics was performed to analyse sEVs derived from $CXCR1^{High}$ cells (HN4) and from $CXCR1^{Low}$ cells (HN6) (Figure 4a, b). In addition, transcriptomic analysis was performed to detect the different expression patterns of HN6 cells, HN4 cells and Cal27 cells treated with or without IL-8 (Figure 4c). Considering that only sEVs derived from $CXCR1^{High}$ cells treated with IL-8 were able to transform $CXCR1^{Low}$ cells, we selected the upregulated proteins in HN4 cell-derived sEVs, and in IL-8 treated HN4 cells and Cal27 cells, and eliminated the differentially expressed products from HN6 cells. The results of Venn diagram analysis identified only one product: ACLY (Figure 4d). ACLY is an upstream regulator of lipid metabolism that catabolizes citrate to produce acetyl CoA and is used as a substrate for lipid synthesis and acetylation modification. Further, Kegg enrichment analysis indicated that the NF-κB p65 pathway was activated, a result that was further confirmed by GSEA analysis (Figure 4b, e).

To verify the above results, we detected the expression of ACLY in IL-8 treated HNSCC cells and found that the level of ACLY was significantly increased in HN4 cells and Cal27 cells, but the difference was not obvious in HN6 cells (Figure 4f). The analysis of sEVs indicated that sEVs produced by $CXCR1^{High}$ cells had more ACLY than those produced by $CXCR1^{Low}$ cells (Figure 4g). Further, we discovered an elevated level of ACLY along with CXCR1 in HN6 cells treated with sEVs produced by $CXCR1^{High}$ cells (Figure 4h). To fully understand the role of ACLY in this process, we regulated its expression in HN6 cells, HN4 cells and Cal27 cells by transfecting plasmids or siRNA targeting ACLY. Considering that the effect of ACLY on lipid metabolism may have an impact on sEVs production, we determined the concentration of sEVs after the transfection. The concentration of sEVs was increased when ACLY was overexpressed whereas knockdown of ACLY decreased its concentration (Figure S3A, B). Therefore, we used the same quality of sEVs to ensure the consistency of each group. After the overexpression of ACLY, CXCR1 was significantly increased in $CXCR1^{Low}$ cells (Figure 4i). Meanwhile, sEVs from the different types of cells were isolated and added to HN6 cells. With the elevated level of ACLY in sEVs after the transfection (Figure 4j), the expression of CXCR1 in HN6 cells was increased even when treated with sEVs derived from $CXCR1^{Low}$ cells (Figure 4k). Conversely, the knockdown of ACLY by siRNA decreased the expression of CXCR1 in HN4 cells and in Cal27 cells (Figure S3C, D), reduced the amount of ACLY in sEVs (Figure S3E, F) and weakened its effect to promote CXCR1 expression (Figure S3G, H). Both si-ACLY-1 and si-ACLY-2 effectively reduced the expression level of ACLY and blocked the transformation of $CXCR1^{Low}$ cells (Figure S3I). For the concise of further exploration, si-ACLY-1 was selected to reduce ACLY levels in subsequent experiments. Moreover, the content of

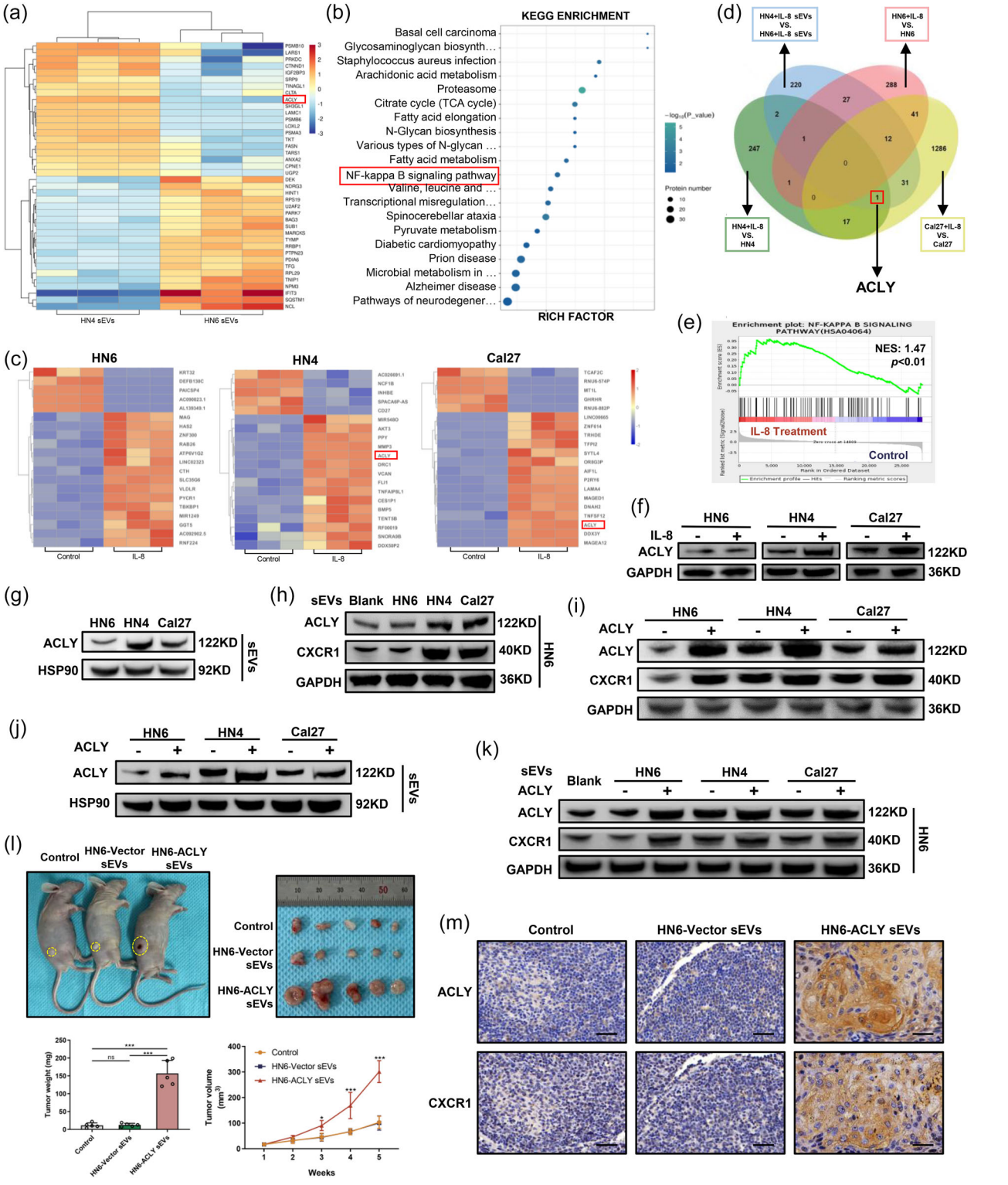

FIGURE 4 **ACLY in sEVs derived from CXCR1^{High} cells regulates the transforming process**. (a) Heatmap displaying the results of LC-MS/MS-based proteomics for sEVs derived from CXCR1^{High} cells (HN4) and from CXCR1^{Low} cells (HN6). (b) Bubble plot showing the pathways predicted by Kegg enrichment analysis. (c) Transcriptomic analysis of different expression patterns in HN6, HN4 and Cal27 cells treated with or without IL-8. (d) Venn diagram analysis of the results of LC-MS/MS-based proteomics and transcriptomic analysis. Intersection of up-regulated genes in HN4 cell-derived sEVs, IL-8 treated HN4 and Cal27 cells eliminated the differential expression products from HN6 cells and identified ACLY. (e) GSEA analysis of the NF-κB p65 pathway with the treatment of IL-8. (f) Western blot showing the expression of ACLY in HNSCC cells after treatment with IL-8 (100 ng/mL). (g) Levels of ACLY in sEVs derived from IL-8-treated CXCR1^{High} cells (HN4, Cal27) and CXCR1^{Low} cells (HN6). (h) Protein level of ACLY and CXCR1 in HN6 cells after treatment with sEVs derived from the indicated cells. (i) ACLY and CXCR1 expression in HNSCC cells transfected with vector or plasmids containing ACLY. (j) Levels of ACLY in sEVs derived from HNSCC cells with or without over-expression of ACLY. (k) Protein level of ACLY and CXCR1 in HN6 cells as control compared with HN6 cells treated with sEVs derived from HNSCC cells over-expressing ACLY as indicated. (l) Representative images, tumour weights and growth curves of

(Continues)

FIGURE 4 (Continued)
xenograft tumours treated with sEVs derived from HN6 cells transfected with vector or plasmids containing ACLY. (m) IHC staining of ACLY and CXCR1 in xenograft tumours derived from the indicated groups. Scale bars, 50 μm. ns, not significant, * $p < 0.05$ and *** $p < 0.001$. Data in (l) were calculated by one-way ANOVA.

CXCR1 in sEVs was barely detectable despite the fact that transfection of plasmids or siRNAs proved that sEVs could not directly transport CXCR1 into $CXCR1^{Low}$ cells (Figure S3J-L). Finally, in vivo assays were used to validate the results shown above. After the injection of sEVs derived from HN6 cells that over-expressed ACLY, the xenograft tumours had a significantly faster growth rate and gradually became larger and heavier (Figure 4l). IHC staining showed that the majority of tumour cells in the HN6-ACLY sEVs-treated tumours eventually had an elevated level of CXCR1 as well as ACLY (Figure 4m). These data proved that ACLY in sEVs derived from $CXCR1^{High}$ cells regulates the transforming process. However, the underlying mechanism behind that process needed further exploration.

3.5 | ACLY acetylates NF-κB p65 to stimulate the expression of CXCR1

To characterize the underlying mechanism of the ACLY regulation of CXCR1 expression, we performed transcriptomic analysis of HNSCC cells transfected with plasmids with or without ACLY. That analysis revealed that the NF-κB p65 pathway was activated (Figure 5a). In accordance with its function, our results showed that the over-expression of ACLY enhanced the production of acetyl CoA (Figure 5b) and the acetylation of p65 (Figure 5c). Based on these results, we assumed that ACLY elevated the level of acetyl CoA to acetylate p65, which then activated the expression of CXCR1. To test that hypothesis, we detected the level of acetyl CoA and acetylated p65 (ac-p65) in HNSCC cells. As we suspected, $CXCR1^{High}$ cells (HN4 and Cal27) had a significantly higher level of acetyl CoA (Figure 5d). Western blot analysis also demonstrated that the expression level of ac-p65 was significantly higher in HN4 cells and Cal27 cells as was ACLY and CXCR1 (Figure 5e). To thoroughly explore this issue, we regulated the expression of ACLY and detected that separately. The over-expression of ACLY led to a significant increase of acetyl CoA as well as ac-p65 and CXCR1 in $CXCR1^{Low}$ cells (HN6) (Figure 5f, g). Similar results were observed using sEVs derived from ACLY-over-expressing cells. The enhancement of ACLY led to an elevated level of acetyl CoA and as well as ac-p65 and CXCR1 in HN6 cells (Figure 5h, i). Conversely, the knockdown of ACLY decreased the level of acetyl CoA along with ac-p65 and CXCR1 even in $CXCR1^{High}$ cells (Figure 5j, k). Likewise, sEVs derived from HN4 cells and from Cal27 cells transfected with si-ACLY lost the ability to increase the level of acetyl CoA, ac-p65 and CXCR1 (Figure 5l, m). The above results indicated that ACLY promotes the production of acetyl CoA to acetylated p65 and increases CXCR1 expression. However, the molecular mechanism of that process is still unclear and it's important to clarify that to stimulate the development of effective targeted drugs.

3.6 | ACLY induces the nuclear translocation of p65 to transcribe CXCR1 via acetylation

The results reported above showed that ACLY promotes p65 acetylation to increase the expression of CXCR1 by producing acetyl CoA. To thoroughly investigate this pathway, we used Bay 11–7082, an inhibitor of the NF-κB pathway to treat HNSCC cells transfected with plasmids containing ACLY. The results showed that inhibition of the NF-κB pathway significantly reduced the enhanced expression of CXCR1 by over-expressing ACLY, indicating that NF-κB was the key pathway in regulating CXCR1 expression (Figure 6a). Next, we proved the critical role of p65 acetylation in CXCR1 expression. Tumour necrosis factor-α (TNF-α) as an activator of the NF-κB pathway was used to stimulate HNSCC cells transfected with si-ACLY. Western blot analysis revealed that without the highly expressed ACLY, TNF-α alone did not increase the expression of CXCR1 (Figure 6b). The knockdown of ACLY reduced the CXCR1 level with or without TNF-α. These results proved that both NF-κB pathway and acetylation enhanced by ACLY are indispensable for CXCR1 expression.

To elucidate how acetylation promotes p65 to transcribe CXCR1, we used immunofluorescence staining to track the location of p65 in HN6 cells treated with sEVs derived from HN4 cells. Immunofluorescence images showed that HN4 cell-derived sEVs significantly improved the translocation of p65 into nucleus (Figure 6c). In this case, we analysed cytoplasmic and nuclear proteins separately. Western blot analysis showed a slight increase of p65 and a significant increase of ac-p65 in nucleus upon stimulation with sEVs derived from $CXCR1^{High}$ cells. The content of ACLY was increased in nucleus, but not as much as in the cytoplasm after treatment with sEVs derived from $CXCR1^{High}$ cells. The level of CXCR1 in the cytoplasm was elevated in HN6 cells treated with HN4- and Cal27-derived sEVs (Figure 6d). To further explore the effect of ACLY on p65, we transfected plasmids contained ACLY into HN6 cells. Immunofluorescence images showed that the level of p65 in the nucleus was significantly increased after the over-expression of ACLY (Figure 6e). Western blot analysis revealed that p65 and ac-p65 were significantly enhanced in nucleus by overexpression of ACLY. As predicted, the expression level of CXCR1 in the cytoplasm also increased (Figure 6f). These results indicated that ACLY facilitates the acetylation of p65 to induce its nuclear translocation and the subsequent transcription

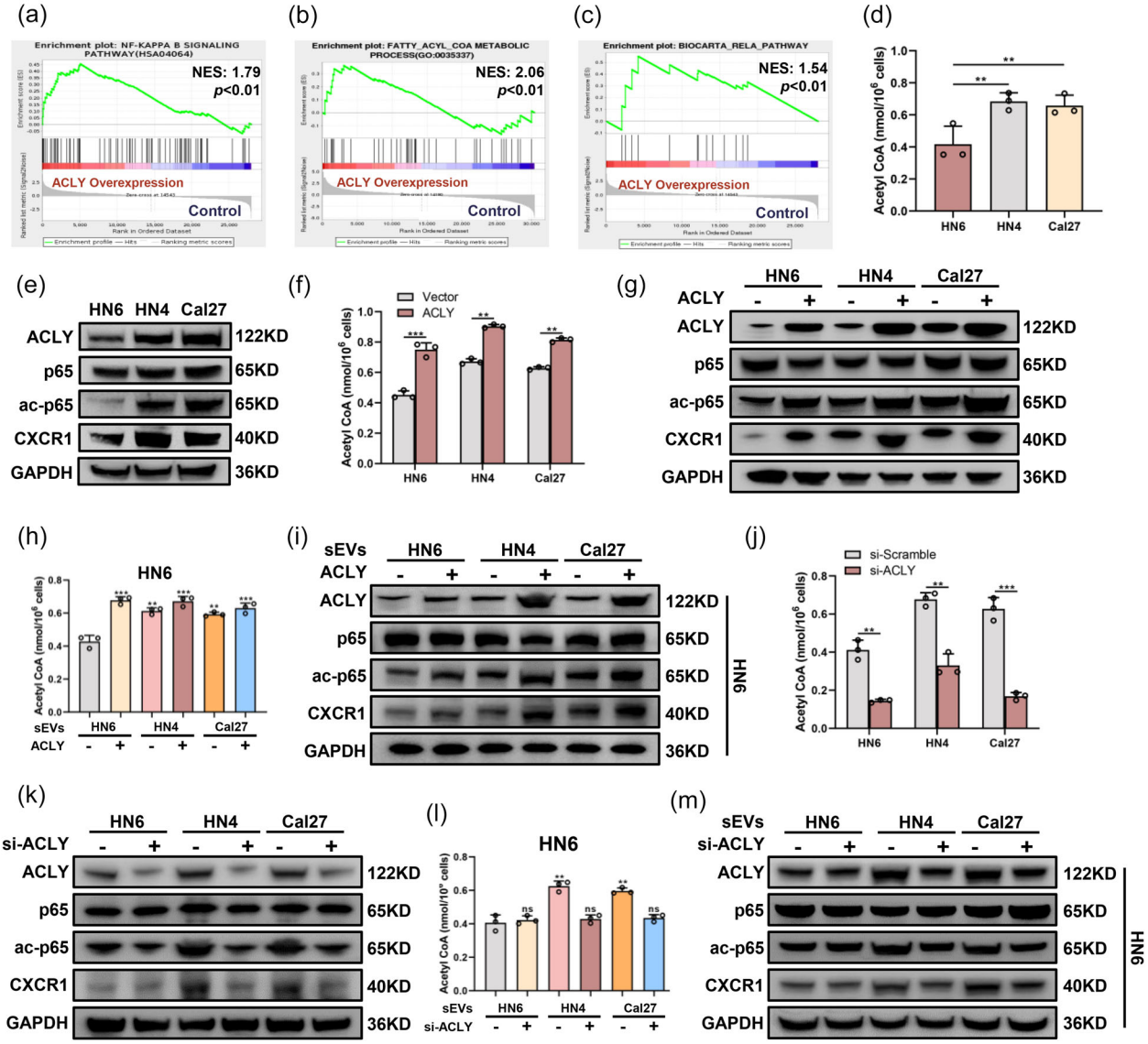

FIGURE 5 **ACLY acetylates NF-κB p65 to stimulate the expression of CXCR1**. (a, b, c) GSEA analysis of the NF-κB p65 pathway, acetyl CoA metabolism and acetylation of NF-κB p65 with over-expression of ACLY. (d, e) Levels of acetyl CoA (d) and ACLY, p65, ac-p65, CXCR1 expression (e) in IL-8-treated $CXCR1^{High}$ cells (HN4, Cal27) and $CXCR1^{Low}$ cells (HN6). (f, g) Analysis of acetyl CoA content (f) and ACLY, p65, ac-p65, CXCR1 expression (g) in HNSCC cells transfected with vector or plasmids containing ACLY. (h, i) Level of acetyl CoA (h) and ACLY, p65, ac-p65, CXCR1 expression (i) in HN6 cells treated with sEVs derived from HNSCC cells transfected with vector or plasmids containing ACLY as indicated. (j, k) Concentration of acetyl CoA (j) and expression level of ACLY, p65, ac-p65 and CXCR1 (k) in HNSCC cells transfected with si-scramble or si-ACLY. (l, m) Levels of Acetyl CoA (l) and ACLY, p65, ac-p65 and CXCR1 (m) in HN6 cells treated with sEVs derived from cells transfected with si-scramble or si-ACLY as indicated. ns, not significant, ** $p < 0.01$, and *** $p < 0.001$. Data in (d, f, j) were calculated by two-tailed unpaired Student's *t*-test; by one-way ANOVA in (h, l).

of CXCR1. Finally, we used the JASPAR dataset to identify the two most likely binding sites of p65 in the promoter region of CXCR1 (Figure 6g). After over-expressing ACLY in HN6 cells, ChIP assays indicated that the binding ability of the −63 to 54 bp region of the CXCR1 promoter to ac-p65 was significantly higher (Figure 6h). This result was confirmed by luciferase assays showing that mutation of Motif2 significantly decreased the luciferase activity compared to the wild-type (Figure 6i).

3.7 | Bempedoic acid targets ACLY to block the transformation of $CXCR1^{Low}$ cells and inhibit the progression of HNSCC

Based on the above results, we concluded that ACLY in sEVs derived from $CXCR1^{High}$ cells mediate the transformation of $CXCR1^{Low}$ cells. This result was further proved in clinical samples. IHC staining and PCR analysis of HNSCC tissue samples showed that there was a significant correlation between CXCR1 and ACLY expression (Figure 7a, b). The TCGA dataset further

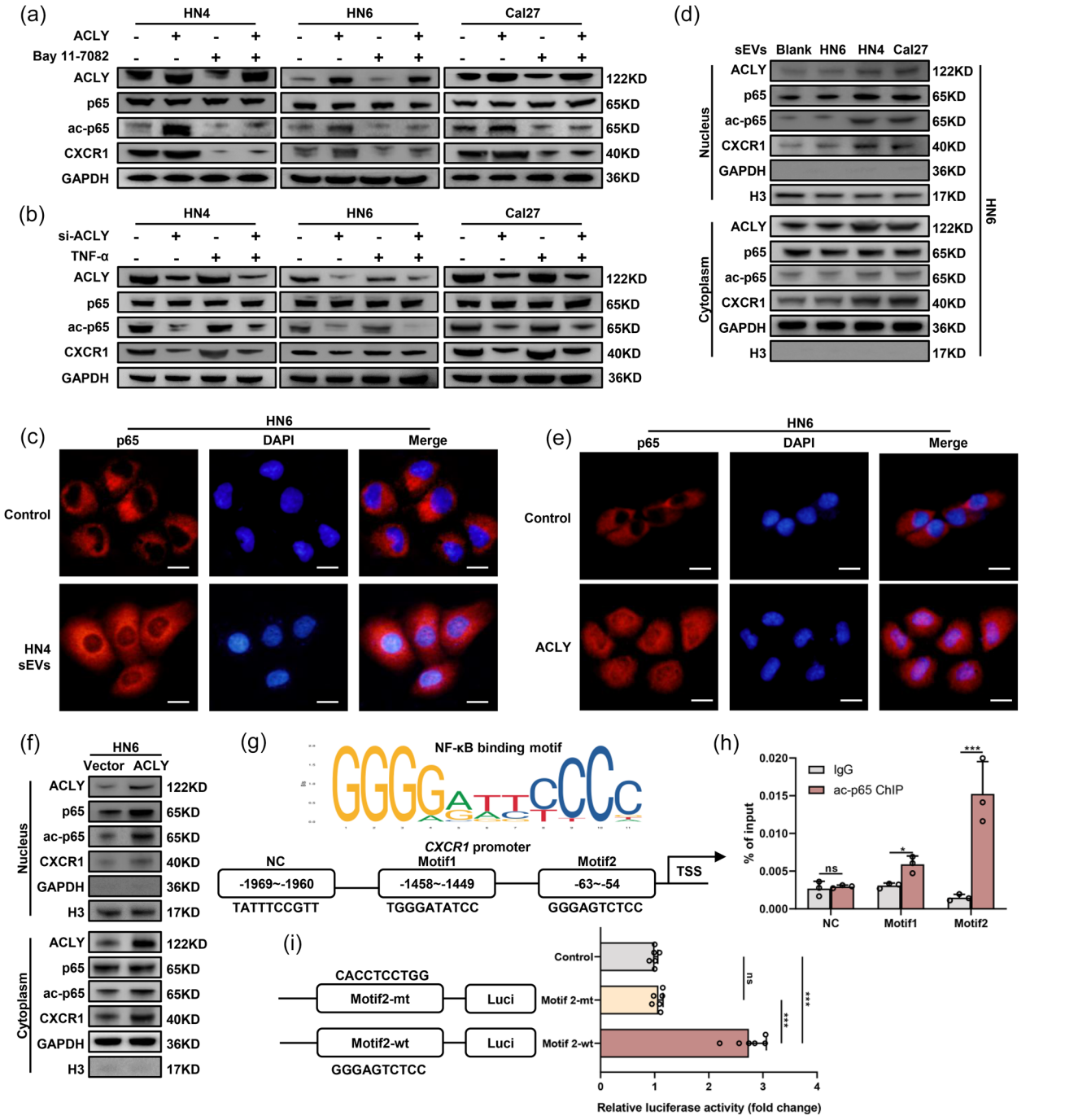

FIGURE 6 **ACLY induces the nuclear translocation of p65 to transcribe CXCR1 via acetylation**. (a) Expression levels of ACLY, p65, ac-p65 and CXCR1 in HN4, HN6 and Cal27 cells transfected with vector or plasmids containing ACLY treated with Bay 11-7082, an inhibitor of the NF-κB pathway, as indicated. (b) Western blot analysis of the expression of ACLY, p65, ac-p65 and CXCR1 in HN4, HN6 and Cal27 cells transfected with si-scramble or si-ACLY treated with TNF-α as indicated. (c) Immunofluorescence images of HN6 cells treated with or without HN4-cell derived sEVs to verify the nuclear translocation of p65. Scale bars, 25 μm. (d) Expression of ACLY, p65, ac-p65 and CXCR1 in the nucleus and cytoplasm were analyzed separately for HN6 cells treated with sEVs derived from $CXCR1^{High}$ cells (HN4, Cal27) and $CXCR1^{Low}$ cells (HN6) as indicated. (e) Immunofluorescence staining was performed to verify the nuclear translocation of p65 after the over-expression of ACLY in HN6 cells. Scale bars, 25 μm. (f) Western blot analysis of ACLY, p65, ac-p65 and CXCR1 in the nucleus and cytoplasm of HN6 cells transfected with vector or plasmids containing ACLY as indicated. (g) Predicted binding site of p65 in the promoter region of CXCR1. (h) ChIP-qPCR analysis of ac-p65 binding on the two predicted motifs in the CXCR1 promoter region in HN6 cells. (i) Dual-luciferase reporter assays performed to validate the binding of p65 to wild-type and mutant Motif 2 in the CXCR1 promoter region. ns, not significant, * $p < 0.05$, and *** $p < 0.001$. Data in (h, i) were calculated by two-tailed unpaired Student's *t*-test.

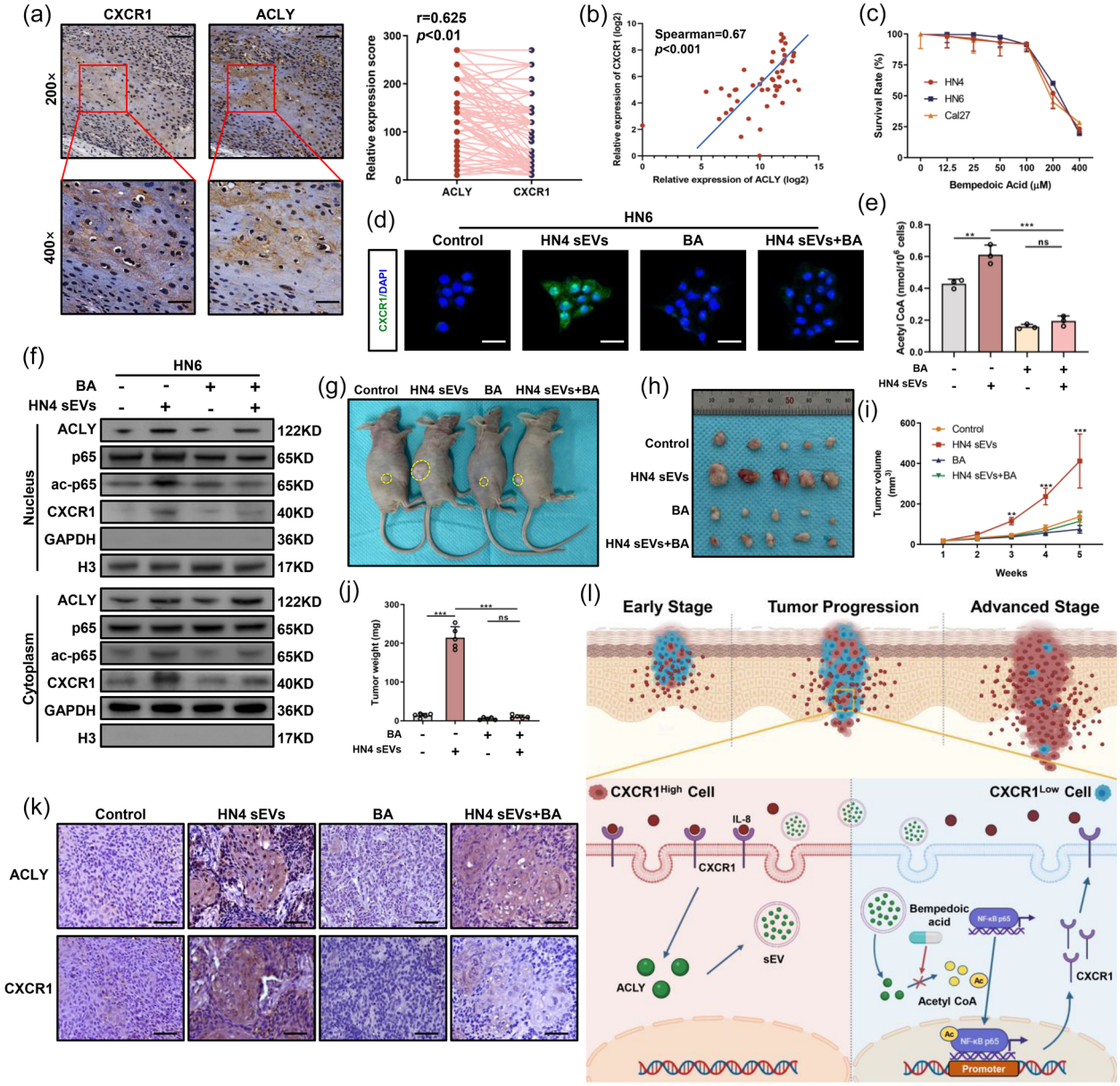

FIGURE 7 **Bempedoic acid targets ACLY to block the transformation of CXCR1^{Low} cells and inhibit the progression of HNSCC.** (a) Representative IHC images and correlation analysis of ACLY and CXCR1 expression from 48 HNSCC tissue samples. Scale bars, 50 μm (top row), 25 μm (bottom row). (b) Correlation analysis of ACLY and CXCR1 based on the HNSCC tissue samples ($n = 48$). (c) Survival analysis of HNSCC cells treated with different concentrations of BA. (d) Immunofluorescence staining for CXCR1 in HN6 cells treated with HN4-derived sEVs and BA (100 μM) for 24 h. Green: CXCR1, Blue: DAPI. Scale bars, 50 μm. (e) Acetyl CoA level in HN6 cells treated with HN4 cell-derived sEVs and BA (100 μM) as indicated. (g) Western blot analysis of ACLY, p65, ac-p65 and CXCR1 in the nucleus and cytoplasm of HN6 cells treated with HN4 cell-derived sEVs and BA (100 μM) as indicated. (g-j) Representative images (g, h), growth curves (i) and tumour weights (j) of xenograft tumours treated with HN4 cell-derived sEVs and BA (30 mg/kg, i.p. once a day) as indicated. (k) IHC staining for ACLY and CXCR1 of xenograft tumours derived from the indicated group. Scale bars, 50 μm. (l) Schematic diagram showing the increased proportion of CXCR1^{High} cells during tumour progression. Mechanistically, sEVs derived from IL-8-activated CXCR1^{High} cells deliver ACLY into CXCR1^{Low} cells to acetylate NF-κB p65 and facilitate its nuclear translocation which transcribes CXCR1 and transforms CXCR1^{Low} cells into CXCR1^{High} cells. ns, not significant, ** $p < 0.01$, and *** $p < 0.001$. Data in (e, i, j) were calculated by two-tailed unpaired Student's t-test.

confirmed the positive correlation of CXCR1 and ACLY (Figure S4A). Moreover, the expression of ACLY was found to be associated with prognosis, tumour stage and lymph node metastasis of HNSCC in clinical samples (Figure S4B-D). Considering the importance of the ACLY-mediated transformation of CXCR1^{Low} cells in the progression of HNSCC, we tried to target ACLY and block that process.

As the only FDA-approved drug that targets ACLY, the effectiveness of BA for HNSCC treatment was unknown. The survival assays confirmed the cytotoxic effect of BA on HNSCC cells and indicated that 100 μM is a suitable concentration of BA to avoid its direct killing effect (Figure 7c). BA and HN4 cell-derived sEVs were applied to HN6 cells for 24 h and the immunofluorescent

staining images showed that BA reduced the transforming effect of CXCR1^{High} cell-derived sEVs (Figure 7d). Further, the level of acetyl CoA which was originally elevated by the stimulation with sEVs derived from CXCR1^{High} cells, could not be increased by the addition of both BA and sEVs derived from HN4 cells (Figure 7e). Western blot analysis showed the same trend. Despite the elevated level of ACLY in cytoplasm after treatment with HN4 cell-derived sEVs, the nuclear translocation of p65 and the expression of ac-p65 in nucleus were significant inhibited by BA, along with the level of CXCR1 in cytoplasm (Figure 7f). Finally, in vivo studies proved these results. The progression of xenograft tumours formed by HN6 cells was originally enhanced by sEVs derived from CXCR1^{High} cells was significantly inhibited by the addition of BA (Figure 7g-j). IHC staining revealed that BA blocked the transformation of CXCR1^{Low} cells even with an elevated level of ACLY (Figure 7k). These results indicated that BA as a targeted drug for ACLY could inhibit the progression of HNSCC by blocking the transformation of CXCR1^{Low} cells. Taken together, this study proved that ACLY in sEVs derived from IL-8-activated CXCR1^{High} cells transform CXCR1^{Low} cells into CXCR1^{High} cells via acetylated NF-κB p65 and facilitated its nuclear translocation (shown schematically in Figure 7l). Thus, we propose a novel "contagion model" in which tumour cells with more active malignant behaviours such as CXCR1^{High} cells can infect "lazy" cells such as CXCR1^{Low} cells via sEVs in the TME and transform them into a more active type. This model proposes that the communication between heterogeneous tumour cells promotes the formation of a dominant subset of cells and stimulates tumour progression.

4 | DISCUSSION

The importance of heterogeneity in tumour progression and in treatment failure has been recognized due to the rapid development of single-cell transcriptomic analysis yet communications between heterogeneous tumour cells are still not completely understood (Choi et al., 2023; Qian et al., 2022). Herein, we report a "contagion model" to describe how CXCR1^{High} cells with higher migration and invasion abilities transform CXCR1^{Low} cells via sEVs into CXCR1^{High} cells to promote the progression of HNSCC.

sEVs function as transport couriers for intercellular substances and have been widely proven to have a significant impact on the TME by inducing metabolic reprogramming, immune evasion, drug resistance and tumour progression (Guo et al., 2022; Rubenich et al., 2021; Zhang & Yu, 2019; Zhong et al., 2023). For example, sEVs secreted by breast cancer cells regulate the metabolic program of cancer-associated fibroblasts (CAFs) to promote tumour progression (Yan et al., 2018). Lu et al. demonstrated that sEVs derived from HNSCC cells could be phagocytosed by tumour-associated macrophages (TAMs) and led to immunosuppression (Lu et al., 2022). Herein, we showed that sEVs can promote tumour progression by inducing the transformation of a less active subset of heterogeneous tumour cells into a more active form. Our conclusion, while confirming the role of sEVs in regulation of the TME, demonstrate for the first time the important regulatory effect of sEVs on the dynamic changes of heterogeneous tumour cells. The contents of sEVs are highly regulated by the cells of origin (Jeppesen et al., 2019). In this case, the differential contents of sEVs provided by heterogeneous host cells are important to convey useful regulatory information. In other words, not all sEVs produced by heterogeneous cells are valuable for regulation. In the current study, we found that sEVs derived from CXCR1-related heterogeneous tumour cells have a significant regulatory effect on tumour cells.

CXCR1 is a receptor for IL-8 that is localized on the surface of the cell membrane and large quantities of IL-8 are present in the TME (Ha et al., 2017; Liu et al., 2016). The IL-8/CXCR1 axis has been proven to play a vital role in tumour progression and is considered to be the next promising molecule for targeted therapy (Corrò et al., 2019; Fousek et al., 2021; Ruffini, 2019). However, due to the wide range of sources of IL-8, it is very difficult to thoroughly eliminate this cytokine in the TME. Therefore, growing attention has been given to its receptor—CXCR1 (Witkowski et al., 2021). The activation of CXCR1 has been shown in many studies to be the initiator of various malignant behaviours in tumour cells (Yang et al., 2021). Wang et al. found that the activation of CXCR1 promotes the progression of gastric cancer by phosphorylated AKT and the ERK1/2 pathway (Wang et al., 2016). Molczyk et al. proposed that CXCR1 is a marker for cancer stem cells and is a therapeutic target for solid tumours (Molczyk & Singh, 2023). In accord with previous research, we found that the expression of CXCR1 increased with the stage of tumour, and CXCR1^{High} cells were shown to have more active malignant behaviours than CXCR1^{Low} cells in this study. The sum of these results indicates that this heterogeneity in CXCR1 expression is essential for tumour progression. In addition, our results revealed that HNSCC has the highest expression level of CXCR1 among the tumours examined, which makes the role of CXCR1 in HNSCC even more important. Interestingly, the proliferation ability of CXCR1^{High} and CXCR1^{Low} cells was not significantly different, which indicates that CXCR1^{High} cells do not constitute the majority of HNSCC cells simply by outgrowing CXCR1^{Low} cells. Although CXCR1 is the specific receptor for IL-8, it's not the only receptor. CXCR2 is another receptor for IL-8, which has 76% homology to CXCR1, but the functional differences between CXCR1 and CXCR2 are not entirely clear. Considering the stimulatory effect of IL-8 on tumour cell proliferation, we speculated that IL-8 promotes the proliferation of tumour cells through the IL-8/CXCR2 axis and facilitates other malignant behaviours mainly through CXCR1 in HNSCC. Moreover, instead of CXCR2, Han et al. found that the knockdown of CXCR1 significantly improves the sensitivity of osteosarcoma cells to chemotherapy (Han et al., 2015). In this case, finding a molecule that mediates the transformation of CXCR1^{Low} cells is critical to inhibit the progression of HNSCC caused by the increased expression of CXCR1 and provides an effective target for therapy. Our study suggests that ACLY in sEVs derived from CXCR1^{High} cells is the pivotal key for this process.

Current studies found that ACLY is the upstream regulatory enzyme of lipid metabolism and catabolizes citrate, one of the major products of the tricarboxylic acid (TCA) cycle, and converts it into acetyl CoA (Feng et al., 2020; Zaidi et al., 2012). This function makes ACLY act as the link between glucose metabolism and lipid metabolism and it becomes an important pro-cancer molecule (Granchi, 2018; Zhao et al., 2016). Icard et al. even regarded ACLY as a central metabolic enzyme in cancer (Icard et al., 2020). Interestingly, acetyl CoA as the product of ACLY has also been called "a central metabolite and second messenger" (Pietrocola et al., 2015). In the metabolic process, acetyl CoA is the major substrate of lipid synthesis (Guertin & Wellen, 2023). Moreover, acetyl CoA is also an important signalling molecule due to its essential role in the acetylation process (He et al., 2023; Wu & Guan, 2022). Emerging evidence proved that the presence of ACLY enhances acetylation by producing acetyl CoA (Carrer et al., 2019). Therefore, the important role of ACLY in intercellular signalling should not be neglected. The results of this study showed that ACLY could transfer signals between cells to regulate CXCR1 expression by acetylizing p65, and proved the role of ACLY as a messenger. In the current study, we found that ACLY-promoted acetylation and NF-κB pathway are essential for the transcriptional regulation of CXCR1. The lack of ACLY or the inhibition of NF-κB pathway would decrease the level of CXCR1. Mechanistically, the acetylation of p65 promoted by ACLY facilitated its nuclear translocation to transcribe CXCR1. Compared with sEVs derived from $CXCR1^{High}$ cells, the transfection of plasmids had a higher efficiency to elevate the level of ACLY, and led to a more significant enhancement of p65 and ac-p65 in the nucleus to transcribe CXCR1, indicating that ACLY was the key protein to regulate this transformation process.

Given the vital role of ACLY in tumour progression, researchers have focused on the regulation and inhibition of ACLY (Batchuluun et al., 2022). Previous studies found that the expression of ACLY is regulated by the AKT pathway (Icard et al., 2020; Wei et al., 2021), which is one of the major downstream targets of IL-8/CXCR1 signalling (Sun et al., 2019). In accord with these results, we also found that activation of the IL-8/CXCR1 axis promoted the expression of ACLY. However, the inhibition of ACLY, especially in cancer treatment, requires more research. Besides its critical role in tumour development, ACLY has also been identified as a pivotal molecule for various metabolic diseases including hypertriglyceridemia, non-alcoholic steatohepatitis, etc (Morrow et al., 2022). To date, BA is the only drug that targets ACLY and has been approved by the FDA that was designed as a lipid-lowering medication, but its effect in tumour treatment remains unclear (Nissen et al., 2023; Pinkosky et al., 2016). Herein, we proved that BA can inhibit the progression of HNSCC by blocking the transformation of $CXCR1^{Low}$ cells. This result indicates that BA is a potential targeted drug for HNSCC treatment.

In conclusion, this study showed the effect of $CXCR1^{High}$ cells to transform $CXCR1^{Low}$ cells. sEVs derived from IL-8-activated $CXCR1^{High}$ cells containing ACLY mediate this process through acetylated p65 to facilitate its nuclear translocation and the subsequent transcription of CXCR1. This transformation could be inhibited by the ACLY-targeted drug BA. However, there are still some issues that need further exploration. For example, we found that BA inhibited the elevated level of CXCR1. Considering the significant effect of the IL-8/CXCR1 axis on immune escape, the combination of BA and immune checkpoint blockade therapy is well worth exploring. Further, the effects of sEVs containing a high level of ACLY on other cells in the TME should be considered. Nevertheless, our findings provide a novel "contagion model" to further understand the dynamic change of heterogeneity that is mediated by sEVs in tumour development and we identify BA as a reliable drug for future targeted-drug therapy.

5 | CONCLUSION

This study proposes a novel "contagion model" to interpret tumour progression caused by the dynamic changes of heterogeneous tumour cells. Specifically, we identified the heterogeneity of CXCR1 in HNSCC tumour cells and found that the expression of CXCR1 in HNSCC increased with tumour progression due to the increasing proportion of $CXCR1^{High}$ cells. $CXCR1^{High}$ cells had stronger abilities for invasion and migration, but not for proliferation compared with $CXCR1^{Low}$ cells. Moreover, upon IL-8-mediated activation, $CXCR1^{High}$ cells transformed $CXCR1^{Low}$ cells into $CXCR1^{High}$ cells through the secretion of sEVs. Mechanistically, sEVs derived from IL-8-activated $CXCR1^{High}$ cells contained a high level of ACLY which acetylated NF-κB p65 in $CXCR1^{Low}$ cells. The acetylation of p65 facilitated its nuclear translocation and the transcription of CXCR1 and transformed $CXCR1^{Low}$ cells into $CXCR1^{High}$ cells to promote the progression of HNSCC. That process could be inhibited by BA as the only FDA-approved ACLY-targeted drug. Overall, this study not only illustrates the underlying molecular mechanism by which ACLY promotes CXCR1 expression, but more importantly, we revealed a new paradigm whereby sEVs derived from tumour cells with more active malignant behaviours infect the weaker subset of tumour cells and transform them into a more active form to promote tumour progression. The significance of this "contagion model" among all types of cancers is worth deeper exploration and provides additional approaches for future diagnosis and treatment of HNSCC.

AUTHOR CONTRIBUTIONS

Qiaoshi Xu: Conceptualization; formal analysis; funding acquisition; investigation; methodology; resources; writing—original draft; writing—review and editing. **Aoming Cheng**: Data curation; investigation; resources; validation; visualization. **Bo Li**: Data curation; formal analysis; investigation. **Xutengyue Tian**: Investigation; resources; software; visualization. **Zhengxue Han**: Conceptualization; project administration; supervision; writing—review and editing. **Zhien Feng**: Conceptualization; project administration; supervision; writing—review and editing.

ACKNOWLEDGEMENTS

This work was supported by the Beijing Stomatological Hospital, Capital Medical University Young Scientist Program (NO.YSP202111), Beijing Municipal Administration of Hospitals' Youth Programme (QML20231507), National Natural Science Foundation of China (82072984), the Beijing Science and Technology Commission (Z221100007422046), Beijing Nova Program (20230484404) and Beijing Hospitals Authority Clinical medicine Development of special funding support (YGLX202338).

CONFLICT OF INTEREST STATEMENT

The authors declare no conflict of interest.

DATA AVAILABILITY STATEMENT

The mass spectrometry proteomics data have been deposited to the ProteomeXchange Consortium (https://proteomecentral.proteomexchange.org) via the iProX partner repository with the dataset identifier PXD048429. RNA-Seq data has been deposited in NCBI GEO under the accession numbers GSE253091.

ORCID

Zhien Feng https://orcid.org/0000-0003-1952-6734

REFERENCES

Attaran, S., & Bissell, M. J. (2021). The role of tumor microenvironment and exosomes in dormancy and relapse. *Seminars in cancer biology*, *78*, 35–44.

Batchuluun, B., Pinkosky, S. L., & Steinberg, G. R. (2022). Lipogenesis inhibitors: Therapeutic opportunities and challenges. *Nature reviews. Drug discovery*, *21*, 283–305.

Carrer, A., Trefely, S., Zhao, S., Campbell, S. L., Norgard, R. J., Schultz, K. C., Sidoli, S., Parris, J. L. D., Affronti, H. C., Sivanand, S., Egolf, S., Sela, Y., Trizzino, M., Gardini, A., Garcia, B. A., Snyder, N. W., Stanger, B. Z., & Wellen, K. E. (2019). Acetyl-CoA metabolism supports multistep pancreatic tumorigenesis. *Cancer Discovery*, *9*, 416–435.

Choi, J. H., Lee, B. S., Jang, J. Y., Lee, Y. S., Kim, H. J., Roh, J., Shin, Y. S., Woo, H. G., & Kim, C. H. (2023). Single-cell transcriptome profiling of the stepwise progression of head and neck cancer. *Nature Communications*, *14*, 1055.

Corrò, C., Healy, M., Engler, S., Bodenmiller, B., Li, Z., Schraml, P., Weber, A., Frew, I., Rechsteiner, M., & Moch, H. (2019). IL-8 and CXCR1 expression is associated with cancer stem cell-like properties of clear cell renal cancer. *The Journal of pathology*, *248*, 377–389.

Cramer, J., Burtness, B., Le, Q., & Ferris, R. (2019). The changing therapeutic landscape of head and neck cancer. *Nature Reviews. Clinical Oncology*, *16*, 669–683.

Dagogo-Jack, I., & Shaw, A. (2018). Tumour heterogeneity and resistance to cancer therapies. *Nature Reviews. Clinical Oncology*, *15*, 81–94.

Dai, J., Su, Y., Zhong, S., Cong, L., Liu, B., Yang, J., Tao, Y., He, Z., Chen, C., & Jiang, Y. (2020). Exosomes: Key players in cancer and potential therapeutic strategy. *Signal Transduction and Targeted Therapy*, *5*, 145.

Feng, X., Zhang, L., Xu, S., & Shen, A. Z. (2020). ATP-citrate lyase (ACLY) in lipid metabolism and atherosclerosis: An updated review. *Progress in Lipid Research*, *77*, 101006.

Fousek, K., Horn, L., & Palena, C. (2021). Interleukin-8: A chemokine at the intersection of cancer plasticity, angiogenesis, and immune suppression. *Pharmacology & Therapeutics*, *219*, 107692.

Granchi, C. (2018). ATP citrate lyase (ACLY) inhibitors: An anti-cancer strategy at the crossroads of glucose and lipid metabolism. *European Journal of Medicinal Chemistry*, *157*, 1276–1291.

Guertin, D. A., & Wellen, K. E. (2023). Acetyl-CoA metabolism in cancer. *Nature Reviews. Cancer*, *23*, 156–172.

Guo, X., Sui, R., & Piao, H. (2022). Tumor-derived small extracellular vesicles: Potential roles and mechanism in glioma. *Journal of Nanobiotechnology*, *20*, 383.

Ha, H., Debnath, B., & Neamati, N. (2017). Role of the CXCL8-CXCR1/2 axis in cancer and inflammatory diseases. *Theranostics*, *7*, 1543–1588.

Han, X., Du, L., Qiao, H., Tu, B., Wang, Y., Qin, A., Dai, K., Fan, Q., & Tang, T. (2015). CXCR1 knockdown improves the sensitivity of osteosarcoma to cisplatin. *Cancer Letters*, *369*, 405–415.

Hanahan, D. (2022). Hallmarks of cancer: New dimensions. *Cancer Discovery*, *12*, 31–46.

Hao, J., Zou, J., Zhang, J., Chen, K., Wu, D., Cao, W., Shang, G., Yang, J. Y. H., Wong-Lin, K., Sun, H., Zhang, Z., Wang, X., Chen, W., & Zou, X. (2023). scSTAR reveals hidden heterogeneity with a real-virtual cell pair structure across conditions in single-cell RNA sequencing data. *Briefings in Bioinformatics*, *24*(2), bbad062.

He, W., Li, Q., & Li, X. (2023). Acetyl-CoA regulates lipid metabolism and histone acetylation modification in cancer. *Biochimica et Biophysica Acta. Reviews on Cancer*, *1878*, 188837.

Icard, P., Wu, Z., Fournel, L., Coquerel, A., Lincet, H., & Alifano, M. (2020). ATP citrate lyase: A central metabolic enzyme in cancer. *Cancer Letters*, *471*, 125–134.

Jeppesen, D. K., Fenix, A. M., Franklin, J. L., Higginbotham, J. N., Zhang, Q., Zimmerman, L. J., Liebler, D. C., Ping, J., Liu, Q., Evans, R., Fissell, W. H., Patton, J. G., Rome, L. H., Burnette, D. T., & Coffey, R. J. (2019). Reassessment of exosome composition. *Cell*, *177*, 428–445.e18.

Jiang, H., Yu, D., Yang, P., Guo, R., Kong, M., Gao, Y., Yu, X., Lu, X., & Fan, X. (2022). Revealing the transcriptional heterogeneity of organ-specific metastasis in human gastric cancer using single-cell RNA Sequencing. *Clinical and Translational Medicine*, *12*, e730.

Johnson, D., Burtness, B., Leemans, C., Lui, V., Bauman, J., & Grandis, J. (2020). Head and neck squamous cell carcinoma. *Nature Reviews. Disease Primers*, *6*, 92.

Kalluri, R., & LeBleu, V. (2020). The biology function and biomedical applications of exosomes. *Science (New York, N.Y.)*, *367*(6478), eaau6977.

Leemans, C. R., Snijders, P. J. F., & Brakenhoff, R. H. (2018). The molecular landscape of head and neck cancer. *Nature Reviews. Cancer*, *18*, 269–282.

Liu, Q., Li, A., Tian, Y., Wu, J. D., Liu, Y., Li, T., Chen, Y., Han, X., & Wu, K. (2016). The CXCL8-CXCR1/2 pathways in cancer. *Cytokine Growth Factor Reviews*, *31*, 61–71.

Lu, T., Zhang, Z., Zhang, J., Pan, X., Zhu, X., Wang, X., Li, Z., Ruan, M., Li, H., Chen, W., & Yan, M. (2022). CD73 in small extracellular vesicles derived from HNSCC defines tumour-associated immunosuppression mediated by macrophages in the microenvironment. *Journal of Extracellular Vesicles*, *11*, e12218.

Ludwig, N., Yerneni, S. S., Azambuja, J. H., Pietrowska, M., Widłak, P., Hinck, C. S., Głuszko, A., Szczepański, M. J., Kärmer, T., Kallinger, I., Schulz, D., Bauer, R. J., Spanier, G., Spoerl, S., Meier, J. K., Ettl, T., Razzo, B. M., Reichert, T. E., Hinck, A. P., & Whiteside, T. L. (2022). TGFβ(+) small extracellular vesicles from head and neck squamous cell carcinoma cells reprogram macrophages towards a pro-angiogenic phenotype. *Journal of Extracellular Vesicles*, *11*, e12294.

Mody, M., Rocco, J., Yom, S., Haddad, R., & Saba, N. (2021). Head and neck cancer. *Lancet (London, England)*, Dec 18; *398*(10318), 2289–2299.

Molczyk, C., & Singh, R. K. (2023). CXCR1: A cancer stem cell marker and therapeutic target in solid tumors. *Biomedicines*, Feb 16; *11*(2), 576.

Morrow, M. R., Batchuluun, B., Wu, J., Ahmadi, E., Leroux, J. M., Mohammadi-Shemirani, P., Desjardins, E. M., Wang, Z., Tsakiridis, E. E., Lavoie, D. C. T., Reihani, A., Smith, B. K., Kwiecien, J. M., Lally, J. S. V., Nero, T. L., Parker, M. W., Ask, K., Scott, J. W., Jiang, L., … Steinberg, G. R. (2022). Inhibition of ATP-citrate lyase improves NASH, liver fibrosis, and dyslipidemia. *Cell Metabolism*, *34*, 919–936.e8.

Nissen, S. E., Lincoff, A. M., Brennan, D., Ray, K. K., Mason, D., Kastelein, J. J. P., Thompson, P. D., Libby, P., Cho, L., Plutzky, J., Bays, H. E., Moriarty, P. M., Menon, V., Grobbee, D. E., Louie, M. J., Chen, C. F., Li, N., Bloedon, L., Robinson, P., … Nicholls, S. J. (2023). Bempedoic Acid and Cardiovascular Outcomes in Statin-Intolerant Patients. *The New England Journal of Medicine*, *388*, 1353–1364.

Pietrocola, F., Galluzzi, L., Bravo-San Pedro, J. M., Madeo, F., & Kroemer, G. (2015). Acetyl coenzyme A: A central metabolite and second messenger. *Cell Metabolism*, *21*, 805–821.

Pinkosky, S. L., Newton, R. S., Day, E. A., Ford, R. J., Lhotak, S., Austin, R. C., Birch, C. M., Smith, B. K., Filippov, S., Groot, P. H. E., Steinberg, G. R., & Lalwani, N. D. (2016). Liver-specific ATP-citrate lyase inhibition by bempedoic acid decreases LDL-C and attenuates atherosclerosis. *Nature Communications*, *7*, 13457.

Puram, S. V., Tirosh, I., Parikh, A. S., Patel, A. P., Yizhak, K., Gillespie, S., Rodman, C., Luo, C. L., Mroz, E. A., Emerick, K. S., Deschler, D. G., Varvares, M. A., Mylvaganam, R., Rozenblatt-Rosen, O., Rocco, J. W., Faquin, W. C., Lin, D. T., Regev, A., & Bernstein, B. E. (2017). Single-cell transcriptomic analysis of primary and metastatic tumor ecosystems in head and neck cancer. *Cell*, *171*, 1611–1624.e24.

Qian, Y., Zhai, E., Chen, S., Liu, Y., Ma, Y., Chen, J., Liu, J., Qin, C., Cao, Q., Chen, J., & Cai, S. (2022). Single-cell RNA-seq dissecting heterogeneity of tumor cells and comprehensive dynamics in tumor microenvironment during lymph nodes metastasis in gastric cancer. *International Journal of Cancer*, *151*, 1367–1381.

Rubenich, D. S., Omizzollo, N., Szczepański, M. J., Reichert, T. E., Whiteside, T. L., Ludwig, N., & Braganhol, E. (2021). Small extracellular vesicle-mediated bidirectional crosstalk between neutrophils and tumor cells. *Cytokine Growth Factor Reviews*, *61*, 16–26.

Ruffini, P. (2019). The CXCL8-CXCR1/2 axis as a therapeutic target in breast cancer stem-like cells. *Frontiers in oncology*, *9*, 40.

Sun, D., Xie, X. P., Zhang, X., Wang, Z., Sait, S. F., Iyer, S. V., Chen, Y. J., Brown, R., Laks, D. R., Chipman, M. E., Shern, J. F., & Parada, L. F. (2021). Stem-like cells drive NF1-associated MPNST functional heterogeneity and tumor progression. *Cell Stem Cell*, *28*, 1397–1410.e4.

Sun, F., Wang, J., Sun, Q., Li, F., Gao, H., Xu, L., Zhang, J., Sun, X., Tian, Y., Zhao, Q., Shen, H., Zhang, K., & Liu, J. (2019). Interleukin-8 promotes integrin $\beta 3$ upregulation and cell invasion through PI3K/Akt pathway in hepatocellular carcinoma. *Journal of Experimental & Clinical Cancer Research: CR*, *38*, 449.

van Niel, G., Carter, D. R. F., Clayton, A., Lambert, D. W., Raposo, G., & Vader, P. (2022). Challenges and directions in studying cell-cell communication by extracellular vesicles. *Nature Reviews Molecular Cell Biology*, *23*, 369–382.

Vathiotis, I. A., Johnson, J. M., & Argiris, A. (2021). Enhancing programmed cell death protein 1 axis inhibition in head and neck squamous cell carcinoma: Combination immunotherapy. *Cancer Treatment Reviews*, *97*, 102192.

Wang, J., Hu, W., Wu, X., Wang, K., Yu, J., Luo, B., Luo, G., Wang, W., Wang, H., Li, J., & Wen, J. (2016). CXCR1 promotes malignant behavior of gastric cancer cells in vitro and in vivo in AKT and ERK1/2 phosphorylation. *International Journal of Oncology*, *48*, 2184–2196.

Wang, X., Guo, J., Yu, P., Guo, L., Mao, X., Wang, J., Miao, S., & Sun, J. (2021). The roles of extracellular vesicles in the development, microenvironment, anticancer drug resistance, and therapy of head and neck squamous cell carcinoma. *Journal of Experimental & Clinical Cancer Research: CR*, *40*, 35.

Wei, X., Shi, J., Lin, Q., Ma, X., Pang, Y., Mao, H., Li, R., Lu, W., Wang, Y., & Liu, P. (2021). Targeting ACLY attenuates tumor growth and acquired cisplatin resistance in ovarian cancer by inhibiting the PI3K-AKT pathway and activating the AMPK-ROS pathway. *Frontiers in Oncology*, *11*, 642229.

Witkowski, P., Wijkstrom, M., Bachul, P., Morgan, K., Levy, M., Onaca, N., Chaidarun, S., Gardner, T., Shapiro, A., Posselt, A., Ahmad, S., Daffonchio, L., Ruffini, P., & Bellin, M. (2021). Targeting CXCR1/2 in the first multicenter, double-blinded, randomized trial in autologous islet transplant recipients. *American Journal of Transplantation*, Nov; *21*(11), 3714–3724.

Wu, Z., & Guan, K. L. (2022). Acetyl-CoA, protein acetylation, and liver cancer. *Molecular Cell*, *82*, 4196–4198.

Xu, Q., Ma, H., Chang, H., Feng, Z., Zhang, C., & Yang, X. (2020). The interaction of interleukin-8 and PTEN inactivation promotes the malignant progression of head and neck squamous cell carcinoma via the STAT3 pathway. *Cell Death & Disease*, *11*, 405.

Yan, W., Wu, X., Zhou, W., Fong, M. Y., Cao, M., Liu, J., Liu, X., Chen, C. H., Fadare, O., Pizzo, D. P., Wu, J., Liu, L., Liu, X., Chin, A. R., Ren, X., Chen, Y., Locasale, J. W., & Wang, S. E. (2018). Cancer-cell-secreted exosomal miR-105 promotes tumour growth through the MYC-dependent metabolic reprogramming of stromal cells. *Nature Cell Biology*, *20*, 597–609.

Yang, F., Zhang, S., Meng, Q., Zhou, F., Pan, B., Liu, F., & Yu, Y. (2021). CXCR1 correlates to poor outcomes of EGFR-TKI against advanced non-small cell lung cancer by activating chemokine and JAK/STAT pathway. *Pulmonary Pharmacology & Therapeutics*, *67*, 102001.

Yin, Y., Liu, B., Cao, Y., Yao, S., Liu, Y., Jin, G., Qin, Y., Chen, Y., Cui, K., Zhou, L., Bian, Z., Fei, B., Huang, S., & Huang, Z. (2022). Colorectal cancer-derived small extracellular vesicles promote tumor immune evasion by upregulating PD-L1 expression in tumor-associated macrophages. *Advanced Science (Weinheim, Baden-Wurttemberg, Germany)*, *9*, 2102620.

Zaidi, N., Swinnen, J., & Smans, K. (2012). ATP-citrate lyase: A key player in cancer metabolism. *Cancer Research*, *72*, 3709–3714.

Zhang, L., & Yu, D. (2019). Exosomes in cancer development, metastasis, and immunity. *Biochimica et Biophysica Acta. Reviews on Cancer*, *1871*, 455–468.

Zhao, S., Torres, A., Henry, R. A., Trefely, S., Wallace, M., Lee, J. V., Carrer, A., Sengupta, A., Campbell, S. L., Kuo, Y. M., Frey, A. J., Meurs, N., Viola, J. M., Blair, I. A., Weljie, A. M., Metallo, C. M., Snyder, N. W., Andrews, A. J., & Wellen, K. E. (2016). ATP-Citrate Lyase Controls a Glucose-to-Acetate Metabolic Switch. *Cell Reports*, *17*, 1037–1052.

Zhong, W., Xiao, Z., Qin, Z., Yang, J., Wen, Y., Yu, Z., Li, Y., Sheppard, N. C., Fuchs, S. Y., Xu, X., Herlyn, M., June, C. H., Puré, E., & Guo, W. (2023). Tumor-derived small extracellular vesicles inhibit the efficacy of CAR T cells against solid tumors. *Cancer Research*, *83*, 2790–2806.

SUPPORTING INFORMATION

Additional supporting information can be found online in the Supporting Information section at the end of this article.

How to cite this article: Xu, Q., Cheng, A., Li, Bo., Tian, X., Han, Z., & Feng, Z. (2024). The small extracellular vesicle-mediated intercellular transformation of $CXCR1^{Low}$ to $CXCR1^{High}$ tumour cells promotes the progression of head and neck squamous cell carcinoma. *Journal of Extracellular Vesicles*, *13*, e12427. https://doi.org/10.1002/jev2.12427